iScience

CellPress
OPEN ACCESS

Article

Seizure-induced neutrophil adhesion in brain capillaries leads to a decrease in postictal cerebral blood flow

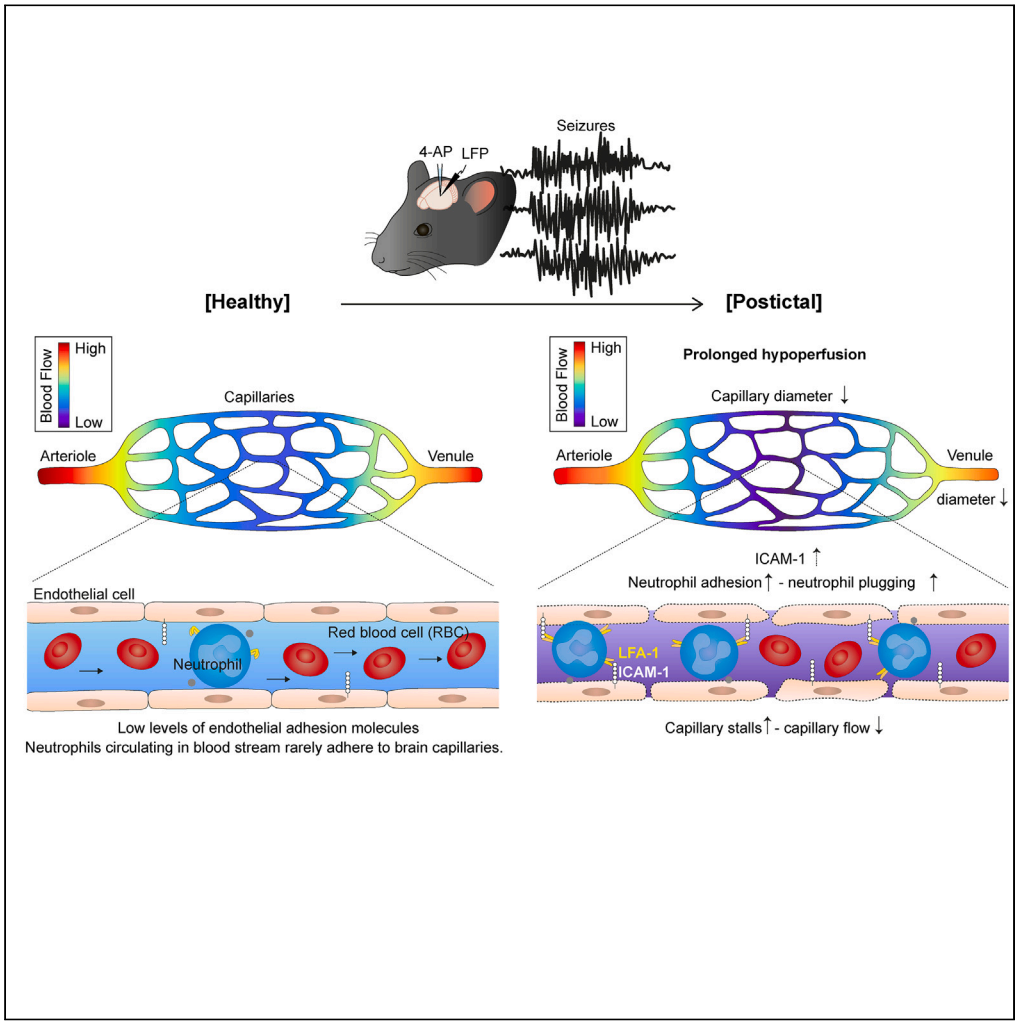

Hyun-Kyoung Lim, Sungjun Bae, Kayoung Han, Bok-Man Kang, Yoonyi Jeong, Seong-Gi Kim, Minah Suh

minahsuh@skku.edu

Highlights

Seizures caused an increased adhesion of neutrophils to brain capillaries

It led to an increased capillary stalling and a prolonged postictal hypoperfusion

The protein level of ICAM-1 was increased in the postictal mouse brains

Administering antibodies against Ly6G and LFA-1 resolved the prolonged hypoperfusion

Lim et al., iScience 26, 106655
May 19, 2023 © 2023
https://doi.org/10.1016/j.isci.2023.106655

iScience

CellPress
OPEN ACCESS

Article

Seizure-induced neutrophil adhesion in brain capillaries leads to a decrease in postictal cerebral blood flow

Hyun-Kyoung Lim,[1,2] Sungjun Bae,[3,4] Kayoung Han,[1,2] Bok-Man Kang,[4] Yoonyi Jeong,[2,3,5] Seong-Gi Kim,[2,3,5] and Minah Suh[1,2,3,4,5,6,7,*]

SUMMARY

Cerebral hypoperfusion has been proposed as a potential cause of postictal neurological dysfunction in epilepsy, but its underlying mechanism is still unclear. We show that a 30% reduction in postictal cerebral blood flow (CBF) has two contributing factors: the early hypoperfusion up to ~30 min post-seizure was mainly induced by arteriolar constriction, while the hypoperfusion that persisted for over an hour was due to increased capillary stalling induced by neutrophil adhesion to brain capillaries, decreased red blood cell (RBC) flow accompanied by constriction of capillaries and venules, and elevated intercellular adhesion molecule-1 (ICAM-1) expression. Administration of antibodies against the neutrophil marker Ly6G and against LFA-1, which mediates adhesive interactions with ICAM-1, prevented neutrophil adhesion and recovered the prolonged CBF reductions to control levels. Our findings provide evidence that seizure-induced neutrophil adhesion to cerebral microvessels via ICAM-1 leads to prolonged postictal hypoperfusion, which may underlie neurological dysfunction in epilepsy.

INTRODUCTION

An adequate blood supply in the brain is fundamental to maintaining normal brain function.[1] Energy substrates, such as glucose and oxygen that are required for brain metabolism are delivered via the bloodstream as a result of proper regulation of cerebral blood flow (CBF). Vascular dysfunction can lead to cellular dysfunction and neuronal degeneration, thus substantially contributing to the pathophysiology of many brain diseases.[2,3] Numerous studies have reported that cerebral hypoperfusion is associated with various brain diseases, including epilepsy.[4–9] In particular, the postictal state following the termination of seizures is frequently accompanied by cerebral hypoperfusion.[10–14]

The postictal state is known to involve an extended period of brain abnormalities such as sensory, cognitive, or motor dysfunction, which can last hours to weeks.[15–18] These abnormalities are not fully explained by neural activity changes, which have been observed to last only a few minutes after seizure offset.[19,20] Case reports have shown that epilepsy patients with postictal brain malfunction present abnormal vascular changes and regional cerebral hypoperfusion.[21–23] Other studies using animal models of epilepsy showed that prolonged hypoxic conditions resulting from hypoperfusion lead to postictal behavior impairments.[10,24] These results indicate that the cause of postictal impairments might be dysfunctional regulation of CBF, considering that an inadequate blood supply could impair brain functions.[2,3] Therefore, understanding the mechanisms underlying seizure-induced vascular changes is important.

Massive neuronal activation in epilepsy is known to induce increased level of excitotoxic substances, and inflammatory cytokines and chemokines in the brain.[25–27] Animal studies have shown that this condition is accompanied by vascular inflammation in the epileptic brain, which involves activation of the cerebral endothelium, with increased expression of leukocyte adhesion molecules.[28,29] These highly expressed adhesion molecules recruit leukocytes from the bloodstream, resulting in augmented leukocyte-endothelial interactions such as neutrophil rolling, adhesion, and trafficking.[30–32] This cascade of events is often followed by degradation of matrix proteins, disruption of blood–brain barrier (BBB) integrity and cellular injury,[2,33–35] which may undermine CBF regulation. Cerebrovascular dysfunction mediated by vascular inflammation may play a detrimental role in impaired CBF regulation in epilepsy. However, this possibility

[1]Biomedical Institute for Convergence at SKKU (BICS), Sungkyunkwan University, Suwon 16419, South Korea

[2]Center for Neuroscience Imaging Research (CNIR), Institute for Basic Science (IBS), Suwon 16419, South Korea

[3]Department of Biomedical Engineering, Sungkyunkwan University, Suwon 16419, South Korea

[4]IMNEWRUN Inc, N Center Bldg. A 5F, Sungkyunkwan University, Suwon 16419, South Korea

[5]Department of Intelligent Precision Healthcare Convergence (IPHC), Sungkyunkwan University, Suwon 16419, South Korea

[6]Samsung Advanced Institute for Health Sciences & Technology (SAIHST), Sungkyunkwan University, Suwon 16419, South Korea

[7]Lead contact

*Correspondence: minahsuh@skku.edu

https://doi.org/10.1016/j.isci.2023.106655

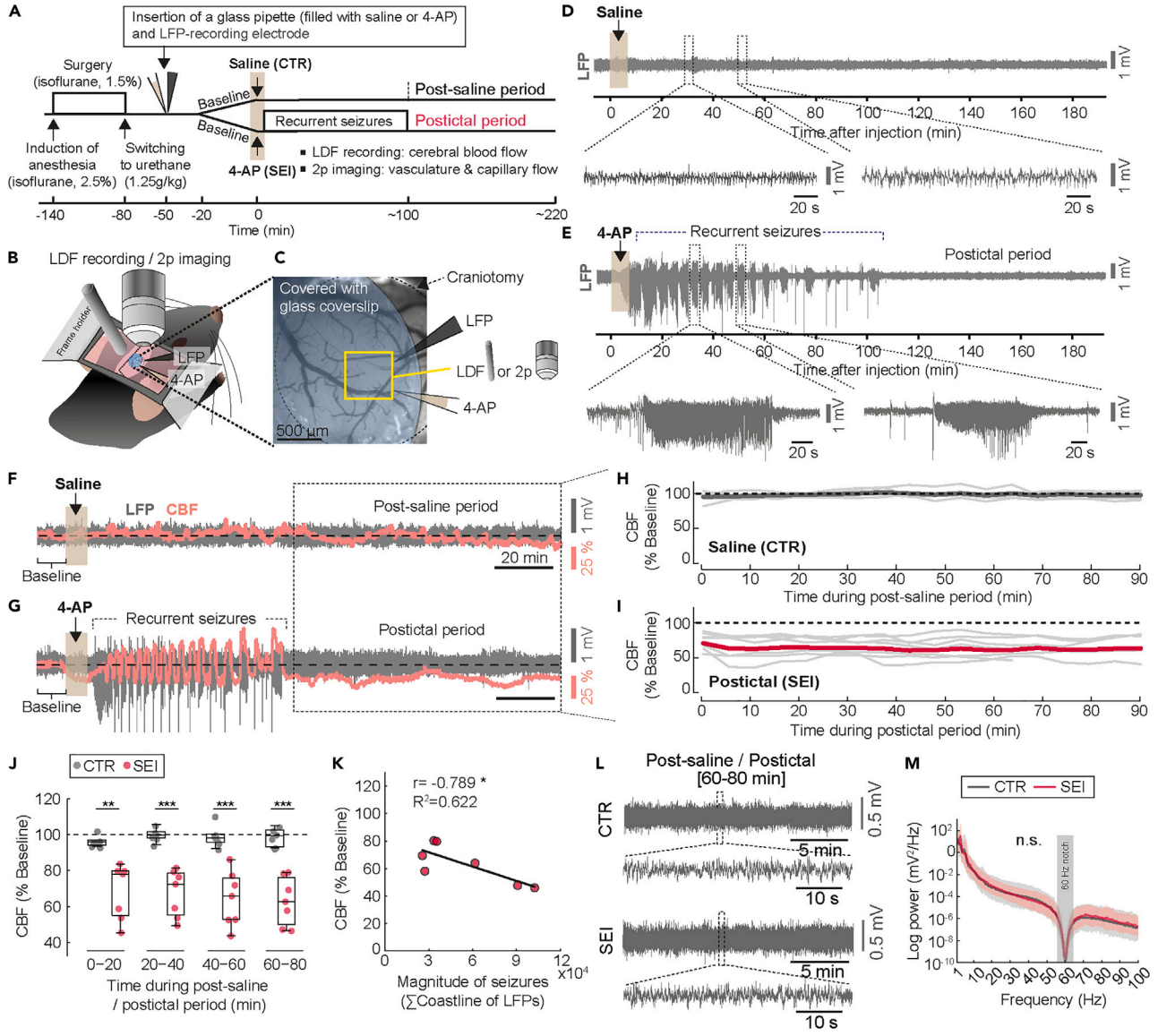

Figure 1. Neural activity and CBF changes during and after recurrent spontaneous seizures induced by 4-AP

(A) Schematic representation of the experimental procedures.

(B) Schematic showing the placement of the LDF recording probe with a 4-AP-filled glass pipette and an LFP recording probe.

(C) Top-view image of the exposed cortex partially covered with a glass cover slip, allowing a space for insertion of the glass pipette and the LFP probe.

(D and E) Examples of LFP traces following intracortical injection of saline (control, CTR) and 4-AP (seizure, SEI) into layer $^{2}/_{3}$ of the somatosensory cortex in mice.

(F and G) Time course traces of LFP signals and CBF changes that were concurrently recorded in saline- and 4-AP-injected mice. CBF signals were normalized to an average of those measured during baseline (% baseline).

(H and I) CBF changes in saline- (CTR: n = 6) and 4-AP (SEI: n = 7) injected animals during post-saline and postictal periods. The time when the last seizure ended (97.82 ± 21.25 min after 4-AP injection, n = 7) was set "0" of the postictal period in individual mice of the SEI group. Comparably, in the CTR group, 90 min after saline injection was set "0" time point of the post-saline period. The average CBF level during 90 min of the post-saline periods in the control group was 98.44 ± 5.33 (% baseline, n = 6). The colored lines represent the averaged trace of individual data, which are depicted by the gray lines.

(J) CBF changes in each 20-min epoch of the post-saline (CTR: n = 6) and the postictal periods (SEI: n = 7). [0–20 min]: 96.44 ± 2.98 (CTR) vs. 68.48 ± 14.27 (SEI), $t_{(6.623)} = 4.678$, **p = 0.003, independent *t* test; [20–40 min]: 99.90 ± 3.43 (CTR) vs. 67.42 vs. 12.08 (SEI), $t_{(7.136)} = 6.287$, ***p = 3.783e^{-4}, independent *t* test; [40–60 min]: 99.29 ± 5.74 (CTR) vs. 64.29 ± 14.17 (SEI), $t_{(8.213)} = 5.527$, ***p = 5.066e^{-4}, independent *t* test; [60–80 min]: 98.66 ± 4.60 (CTR) vs. 62.94 ± 12.42 (SEI), $t_{(7.882)} = 6.526$, ***p = 1.955e^{-4}, independent *t* test.

(K) Scatter plot showing the relationship between the magnitude of preceding seizures and the 60–90 min postictal CBF changes (Pearson's $r = -0.789$, *p = 0.035, $R^2 = 0.622$, n = 7). The magnitude of seizures was calculated by summating coastline lengths (the absolute values of distances from one data point to the next)[37,38] in LFP traces during recurrent seizures.

Figure 1. *Continued*

(L) Examples of LFPs during 60–80 min of the post-saline and the postictal periods.

(M) Power spectra of LFPs recorded during 60–80 min of the post-saline and the postictal periods (CTR: n = 8; SEI: n = 9). "n.s." indicates no statistical significance. Delta (1–4 Hz): $t_{(15)} = -0.003$, p = 0.998, independent *t* test; theta (4–8 Hz): $U_{(8,9)} = 32$, p = 0.7, Mann-Whitney *U* test; alpha (8–14 Hz): $U_{(8,9)} = 32$, p = 0.7, Mann-Whitney *U* test; beta (14–30 Hz): $U_{(8,9)} = 34$, p = 0.847, Mann-Whitney *U* test; gamma (30–100 Hz): $t_{(15)} = 0.401$, p = 0.694, independent *t* test.

has not yet been thoroughly investigated, and how it is linked to cerebral hypoperfusion in epilepsy remains unclear.

In this study, we sought to investigate seizure-induced microvasculature changes and uncover the underlying cellular basis for this phenomenon from the perspective of vascular inflammation. A 4-aminopyridine (4-AP) seizure model was used as previously reported,[36] which allowed us to fully explore the neurovascular dynamics during and after recurrent seizures with a spatially defined focus. We considered this model to be suitable for investigating the effects of seizures on microvascular dynamics and structural changes in a localized brain area.

RESULTS

A prolonged decrease in CBF following the offset of seizure activities

We first investigated the dynamics of CBF with seizure activities via concurrent recordings of laser doppler flowmetry (LDF) and local field potential (LFP) signals in a mouse seizure model (Figures 1A–1C). Electrographic seizures were induced by intracortical 4-AP injection and were maintained for ~100 min (Figure 1E). Notably, CBF was decreased for over an hour after the end of recurrent seizures (Figure 1G). To quantify CBF changes in individual mice where the duration of seizures was variable, the time after termination of the last seizure was defined as the beginning of the "postictal period," which was 97.82 ± 21.25 min on average (n = 7) after seizure induction. During the postictal period, CBF levels were reduced to 66.44 ± 14.12% during the 90-min postictal period (n = 7, Figure 1I) compared to those measured during the baseline period. Meanwhile, saline injection as a sham control did not induce any apparent neural activity changes (Figure 1D) or CBF changes (Figures 1F and 1H). Considering the average duration of recurrent seizures, the beginning of the "post-saline period" in the control group was defined as starting 90 min after saline injection. The postictal CBF was significantly lower than that of control mice (Figure 1J). Both the saline-injected and the 4-AP-injected mice maintained stable anesthesia conditions with a normal range of physiological parameters, including heart rate (Figure S1).

We then examined whether the CBF reductions were related to the magnitude of preceding seizure activities. Coastline lengths of LFP signals during the seizures, which are the absolute values of the distances from one data point to the next,[37,38] were summed and then compared with the averages of CBF levels during the 60–90 min postictal period. These parameters showed a negative linear relationship (Figure 1K), indicating that a higher magnitude of seizures was associated with a greater CBF reduction during the postictal period. LFP power spectra measured during the postictal period did not show any noticeable differences compared to the control group (Figures 1L and 1M; see also Figure S2), implying that the prolonged CBF decrease was not associated with neural activity changes.

We next investigated whether arteriole diameter changes may underlie the postictal CBF changes. Immediately after the offset of the last seizure, surface arteriolar diameters were reduced to 82.94 ± 18.11% (Figures S3B and S3D), compared to those measured during the baseline period, while surface arteriole diameters were almost the same in the control group (102.60 ± 6.23%, Figures S3A and S3C). The postictal surface arteriolar diameters increased gradually over time and almost recovered to baseline levels at 40 min into the postictal period (102.57 ± 15.39%, Figure S3E). We concluded that the postictal CBF reduction was not fully explained by arteriolar constriction and that changes in other vessel components may result in prolonged postictal CBF reductions.

Reduced diameter and stalled blood flow in capillaries during the postictal period

To examine the changes in different vessel components that may underlie prolonged postictal CBF reductions, we conducted a detailed investigation of the cortical microvasculature by using *in vivo* two-photon fluorescence microscopy. We first measured capillary diameter changes after an hour of the postictal period, at which point the CBF reductions persisted with no arteriolar constriction. In control mice, saline injection did not induce any significant changes in vessel diameter (Figures 2A, 2C, 2E, and 2F). Pial and

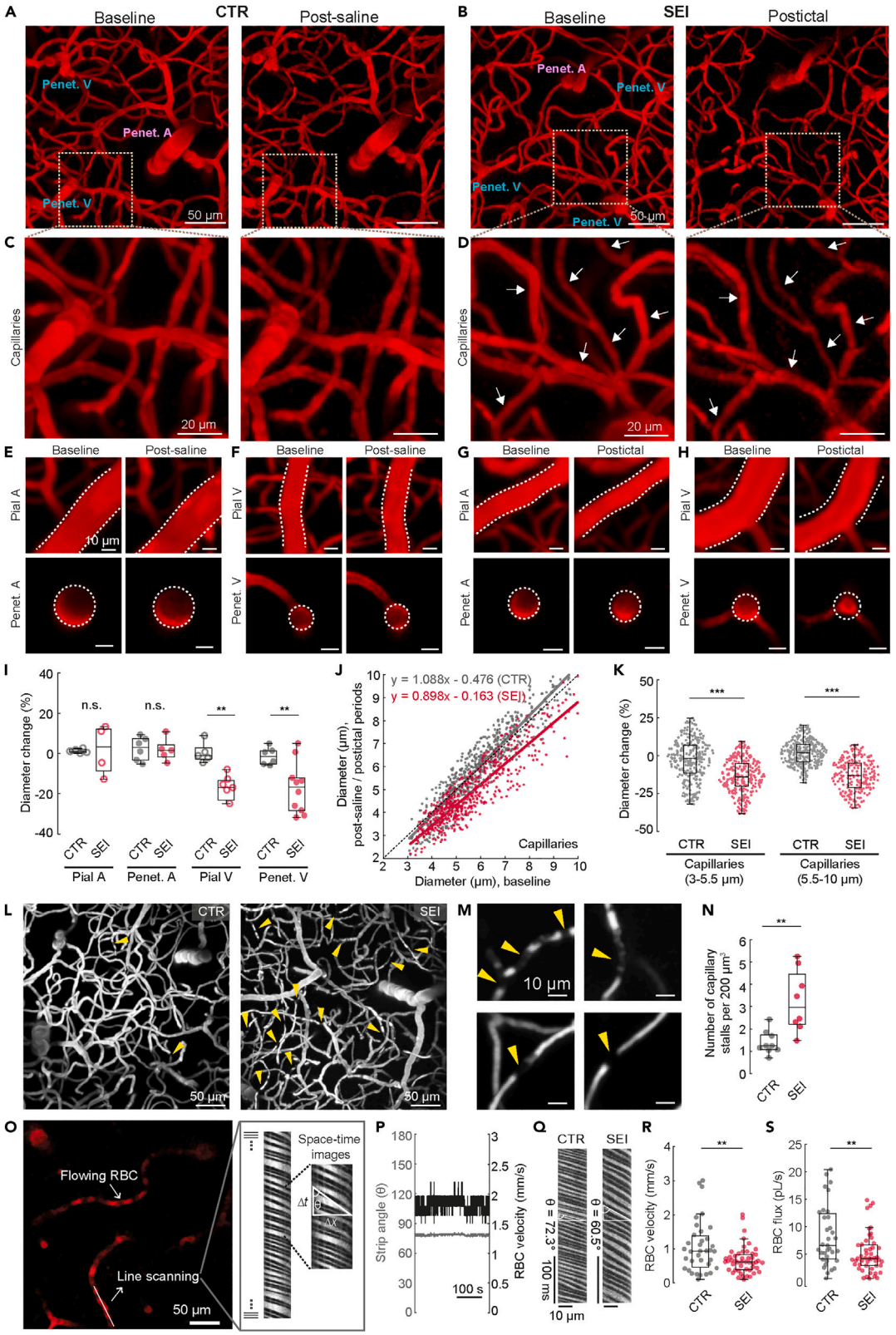
A
Baseline
CTR
Post-saline
B
Baseline
SEI
Postictal
Penet. V
Penet. A
Penet. V
50 μm
C
D
Capillaries
20 μm
E
F
G
H
Baseline
Post-saline
Baseline
Postictal
Pial A
Pial V
Penet. A
Penet. V
10 μm
I
Diameter change (%)
n.s.
n.s.
**
**
CTR
SEI
Pial A
Penet. A
Pial V
Penet. V
J
y = 1.088x - 0.476 (CTR)
y = 0.898x - 0.163 (SEI)
Diameter (μm), post-saline / postictal periods
Diameter (μm), baseline
Capillaries
K
Diameter change (%)
***
***
Capillaries (3-5.5 μm)
Capillaries (5.5-10 μm)
L
CTR
SEI
50 μm
M
10 μm
N
Number of capillary stalls per 200 μm²
O
Flowing RBC
Line scanning
50 μm
Space-time images
P
Strip angle (θ)
RBC velocity (mm/s)
100 s
Q
θ = 72.3°
θ = 60.5°
100 ms
10 μm
R
RBC velocity (mm/s)
S
RBC flux (pL/s)

Figure 2. *In vivo* two-photon vessel imaging during the post-saline and the postictal periods

(A and B) Representative two-photon z stack projection vasculature images up to ~220 μm excluding the pial surface, obtained during the post-saline (CTR) and the postictal (SEI) period. Penet. A: penetrating arteriole, Penet. V: penetrating venule. Scale bar: 50 μm

(C and D) Magnified images of the areas indicated by dotted squares in (A) and (B), showing capillaries in baseline and the post periods. Scale bar: 20 μm

(E–H) Examples of pial and penetrating arterioles, and pial and penetrating venules, in baseline and the post periods. Pial A: pial arteriole, Penet. A: penetrating arteriole, Pial V: pial venule, Penet. V: penetrating venule. Scale bar: 10 μm

(I) Pial and penetrating vessel diameter changes (%) during the post periods, compared to the baseline (CTR: n = 3, pial arteriole n = 5, penetrating arteriole n = 6, pial venule n = 5, penetrating venule n = 6; SEI: n = 4, pial arteriole n = 4, penetrating arteriole n = 5, pial venule n = 7, penetrating venule n = 10). [Pial A]: 1.26 ± 0.91% (CTR) vs. 1.79 ± 10.86% (SEI), $t_{(3.031)} = -0.084$, p = 0.938, independent *t* test; [Penet. A]: 2.66 ± 5.33% (CTR) vs. 2.13 ± 5.13% (SEI), $t_{(9)} = 0.151$, p = 0.883, independent *t* test. "n.s." indicates no statistical significance. [Pial V]: 0.20 ± 4.59% (CTR) vs. −19.82 ± 9.97% (SEI), $t_{(10)} = 3.820$, **p = 0.003, independent *t* test; [Penet. V]: −1.64 ± 3.99% (CTR) vs. −17.41 ± 12.18% (SEI), $t_{(11.999)} = 3.556$, **p = 0.004, independent *t* test.

(J) Plot of capillary diameters during baseline versus the post-saline or postictal periods (CTR: n = 3, vessel segment n = 667; SEI: n = 4, vessel segment n = 522).

(K) Plot of diameter changes in capillary segments that were 3–5.5 μm and 5.5–10 μm when measured during the baseline periods. CTR: n = 3; 3–5.5 μm: vessel segment n = 287, 5.5–10 μm: vessel segment n = 380; SEI: n = 4; 3–5.5 μm: vessel segment n = 290, 5.5–10 μm: vessel segment n = 232. [3-5.5 μm]: −2.75 ± 13.39% (CTR) vs. −13.68 ± 10.97 (SEI), $U_{(287,290)} = 22{,}143$, ***p = $2.355e^{-22}$, Mann-Whitney *U* test; [5.5-10 μm]: 2.25 ± 8.33% (CTR) vs. −12.69 ± 10.35% (SEI), $U_{(380,232)} = 12{,}088$, ***p = $2.354e^{-51}$, Mann-Whitney *U* test.

(L) Representative two-photon z stack projection images (~100–300 μm below the pial surface) showing capillary segments either stalled (yellow arrowheads) or patent in the two groups.

(M) Z-projection of image stacks through stalled capillaries. Scale bar: 10 μm

(N) Quantification of capillary stalls in the CTR (n = 9) and the SEI (n = 8) groups. 1.39 ± 0.49 (CTR) vs. 3.25 ± 1.29 (SEI), $t_{(8.747)} = -3.592$, **p = 0.006, independent *t* test.

(O and P) Line-scan imaging on a capillary segment to acquire space-time images of flowing red blood cells (RBCs). The x axis representing the distance traveled by the RBCs, Δx, and the y axis representing time, Δt. RBC velocity can be calculated from the slope of the RBC streaks (Δx/Δt).

(Q) Representative line-scan images acquired during the post-saline (CTR) and the postictal (SEI) periods.

(R and S) RBC velocity and RBC flux (CTR: n = 8, capillary segments n = 35; SEI: n = 8, capillary segments n = 49). [RBC velocity]: 1.06 ± 0.75 (CTR) vs. 0.67 ± 0.40 (SEI), $U_{(35,49)} = 573$, **p = $9.844e^{-3}$, Mann-Whitney *U* test; [RBC flux]: 8.83 ± 6.41 (CTR) vs. 5.13 ± 3.54 (SEI), $U_{(35,49)} = 543$, **p = 0.004, Mann-Whitney *U* test.

penetrating arterioles measured in the postictal period did not show apparent changes in vessel diameter (Figures 2B, 2G, and 2I; see also Figure S4A). On the other hand, the capillary diameters were reduced during the postictal period (Figures 2D and 2J). Capillaries were further divided into two groups with a threshold of 5.5 μm diameter[39] to examine whether the changes observed in capillaries were size dependent. Both groups of capillaries (3–5.5 μm and 5.5–10 μm) showed reductions in vessel diameter in the postictal group, compared to the control group (Figure 2K). The diameters of the venules were also decreased in the postictal group (Figure 2I; see also Figure S4B). Cortical vessels showed distinct diameter changes at different branch orders (Figure S4C). Vessel of fourth or more branching order from the closest penetrating arterioles and those close to penetrating venules showed significant reductions in vessel diameters (Figure S4D). These results indicate that the postictal CBF reductions were associated with capillary diameter changes, including those on the venular side, but not with arteriolar diameter changes.

Furthermore, along with reduced diameters, capillary segments during the postictal period showed increased stalling (Figure 2L) with different types of obstructions (Figure 2M), which were associated with RBCs, leukocytes, and platelets.[40–42] A number of stalled capillary segments were observed with a cell-sized clog of ~10 μm in diameter (Figure 2M). The number of capillary stalls was 2.34-fold higher than that of the control group (Figure 2N). We then examined whether the increased capillary stalling was associated with blood flow changes in capillaries. RBC velocity was measured by acquiring line-scan images on a flowing capillary segment (Figure 2O) and was then calculated from strip angles of the images (Figure 2P). The postictal group showed significant decreases in RBC velocity (Figures 2Q and 2R) and RBC flux (Figure 2S). The average velocity and flux were 63.31% and 58.11%, respectively, of those measured in the control group. Collectively, these results show that sustained postictal CBF reductions were associated with obstructed capillary flow due to increased capillary stalling, involving reduced capillary diameter.

Neutrophil clogging was a main contributor to increased capillary stalling during the postictal period

We then sought to identify the main contributor to the increased capillary stalling. Given that the postictal capillary stalling was observed to involve cell-sized clogs, leukocytes circulating in the blood vessels were considered potential candidates. It was reported that plugging by neutrophils, which is a subtype of leukocytes and the most abundant, increased capillary stalling in Alzheimer's disease (AD) and ischemic stroke models.[40–43] To confirm that the increased capillary stalling during the postictal period was associated with

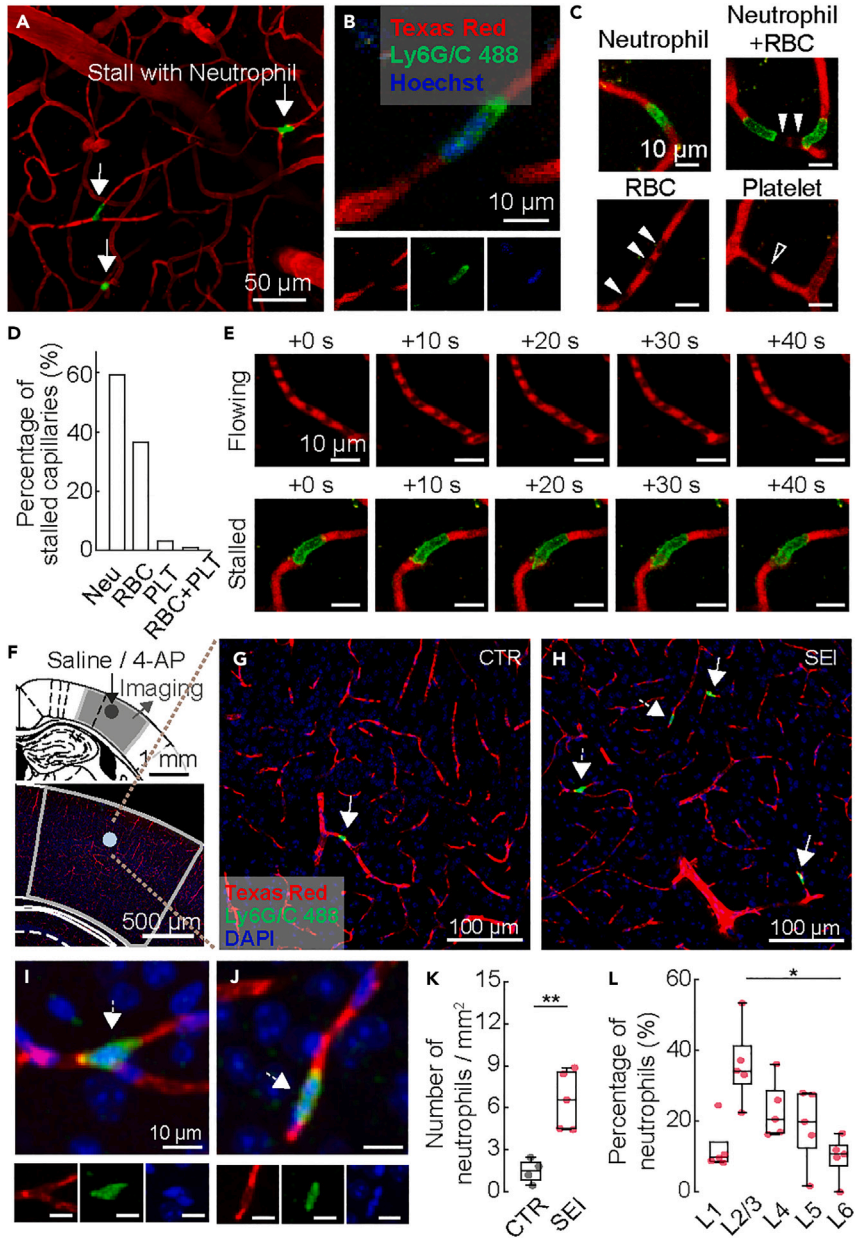

Figure 3. Capillary stalling by neutrophils

(A) Two-photon projection image showing an anti-Ly6C/G (Gr-1)-labeled cell in stalled capillaries.

(B) Magnified image showing a stalled capillary that contained a neutrophil (red: Texas Red-labeled blood plasma; green: neutrophils labeled by anti-Ly6G/C (Gr-1)-Alexa 488 antibody; blue: cell nuclei stained by Hoechst 33342).

(C) Different types of capillary stalling that contained a neutrophil, neutrophil and RBCs, only RBCs, or platelets. Scale bar: 10 μm

(D) Percentage of capillary stalling of the postictal periods (n = 4, 96 stalled capillaries). Neu: capillary stalling that contained a neutrophil or a neutrophil with red blood cell (RBC) or platelet; RBC: capillary stalling only with RBC; PLT: capillary stalling only with platelet; RBC+PLT: capillary stalling that contained both RBC and platelet.

(E) Representative images of capillary segments either patent or stalled with a neutrophil (red: Texas Red-labeled blood plasma; green: a neutrophil labeled by anti-Ly6G/C (Gr-1)-Alexa 488 antibody. Scale bar: 10 μm

(F) Confocal imaging of a fixed brain that was extracted during the post-saline or the postictal period, following injection of Texas Red-conjugated lysine-fixable dextran and Alexa Fluor 488-conjugated Ly6C/G (Gr-1) antibody.

(G and H) Representative images showing stalled capillaries that contained anti-Ly6C/G (Gr-1)-labeled cells in the CTR and the SEI mice.

Figure 3. *Continued*

(I and J) Magnified images of capillaries containing neutrophils, marked as dashed arrows in (H) (red: Texas Red-labeled blood plasma; green: neutrophils labeled by anti-Ly6G/C (Gr-1)-Alexa 488 antibody; blue: cell nuclei stained by DAPI). Scale bar: 10 μm

(K) Quantification of neutrophil plugs in capillaries (CTR: n = 4; SEI: n = 5; Counted numbers in two or three brain slices were averaged in each animal). 1.49 ± 0.73 (CTR) vs. 6.57 ± 1.87 (SEI), $t_{(7)} = -4.452$, **p = 0.003, independent *t* test.

(L) Percentage of neutrophil plugs in different cortical layers (layer 1: 12.36 ± 6.09%, layer 2/3: 36.04 ± 9.98%, layer 4: 23.17 ± 7.33%, layer 5: 18.62 ± 9.62%, layer 6: 9.80 ± 5.42%, $\chi^2(4) = 13.868$, p = 0.008, Kruskal-Wallis *H* test with Mann-Whitney *post hoc* comparisons (* indicates p < 0.005, Bonferroni-corrected).

neutrophils, we visualized neutrophils by using an Alexa 488-conjugated Ly6C/G (Gr-1) antibody[44] in the postictal vasculature. The data revealed that a number of stalled capillary segments contained neutrophils (Figures 3A–3C), i.e., a total of 59.38% of the capillary stalls measured during the postictal period were associated with neutrophils (Figure 3D). Segments stalled by neutrophils were generally maintained for more than a few tens of seconds (Figure 3E).

Neutrophil clogging over a wide range of areas around seizure foci and throughout cortical layers was further examined in fixed mouse brains (Figure 3F). The postictal group (SEI) showed a significantly increased number of neutrophil plugs in capillary segments compared to those observed in the control group (CTR) (Figures 3G–3K). The proportion of neutrophil clogs was relatively high in layers 2/3, where seizures were induced (Figure 3L). We concluded that neutrophil plugging of capillaries was increased by seizures, thus resulting in increased capillary stalling during the postictal period.

The postictal decrease in CBF was resolved by the administration of an anti-Ly6G antibody targeting neutrophils

We next examined whether increased capillary stalling induced by neutrophil plugging was a main cause of the sustained postictal CBF decrease. We administered antibodies against Ly6G, which is a neutrophil-specific marker,[45] since the antibodies were shown to mitigate the capillary stalling observed in the context of AD and ischemic stroke by preventing neutrophil adhesion to capillaries.[41–43] Anti-Ly6G (αLy6G) or its control isotype (cIgG) antibody was administered intravenously 40 min before the induction of seizures (Figure 4A). Antibody injection did not induce changes in physiological parameters such as heart rate (Figure 4B), which maintained stable throughout the experiments (Figure S5). The CBF level changed immediately after the antibody injection, but it returned to baseline levels within 30 min (Figure 4C). Anti-Ly6G and isotype antibodies did not alter the magnitude or duration of recurrent seizures (Figures 4D–4F). The neural activities shown by LFP power spectra were also similar between the two groups during the postictal periods (Figures 4G and 4H; see also Figure S6).

Interestingly, the anti-Ly6G antibody-treated group (Figure 4I, αLy6G + SEI) showed a recovery of CBF, while the prolonged CBF decrease was maintained in the isotype antibody-treated group (Figure 4I, cIgG+SEI). The CBF levels in the anti-Ly6G group were significantly higher from 40 min into the postictal period than those in the isotype group and recovered to the baseline level at 60–80 min (Figure 4J). The postictal CBF at 60–90 min in the anti-Ly6G group did not show a linear relationship with the magnitude of seizures due to CBF recovery, while the linear relationship was maintained in the control isotype group (Figure 4K).

We then compared the dynamics of arteriolar diameter to those observed in the CBF recovery. In the anti-Ly6G group, arteriolar constrictions were also observed during the early phase of the postictal period (Figures S7B and S7D), and the arteriolar diameters gradually recovered to the baseline diameters within an hour (Figure S7E), which was consistent with CBF recovery (Figures 4I and 4J, αLy6G + SEI). In the isotype group, the dynamics of arteriolar changes were similar (Figures S7A, S7C, and S7E), but the CBF reductions persisted throughout the postictal period (Figures 4I and 4J, cIgG+SEI). These results imply that changes in different vessel components can differentially contribute to postictal CBF reductions over time. Collectively, we concluded that the postictal CBF change during the early phase was predominantly affected by arteriolar constriction, but the CBF reductions that persisted for an extended period of time were due to neutrophils.

Effects of anti-Ly6G antibody treatment on the microvasculature and capillary stalling during the postictal period

We next aimed to confirm the vascular changes underlying the improvement in postictal CBF induced by anti-Ly6G antibody treatment. In both the isotype (Figure 5A) and anti-Ly6G (Figure 5B) groups, the arteriolar

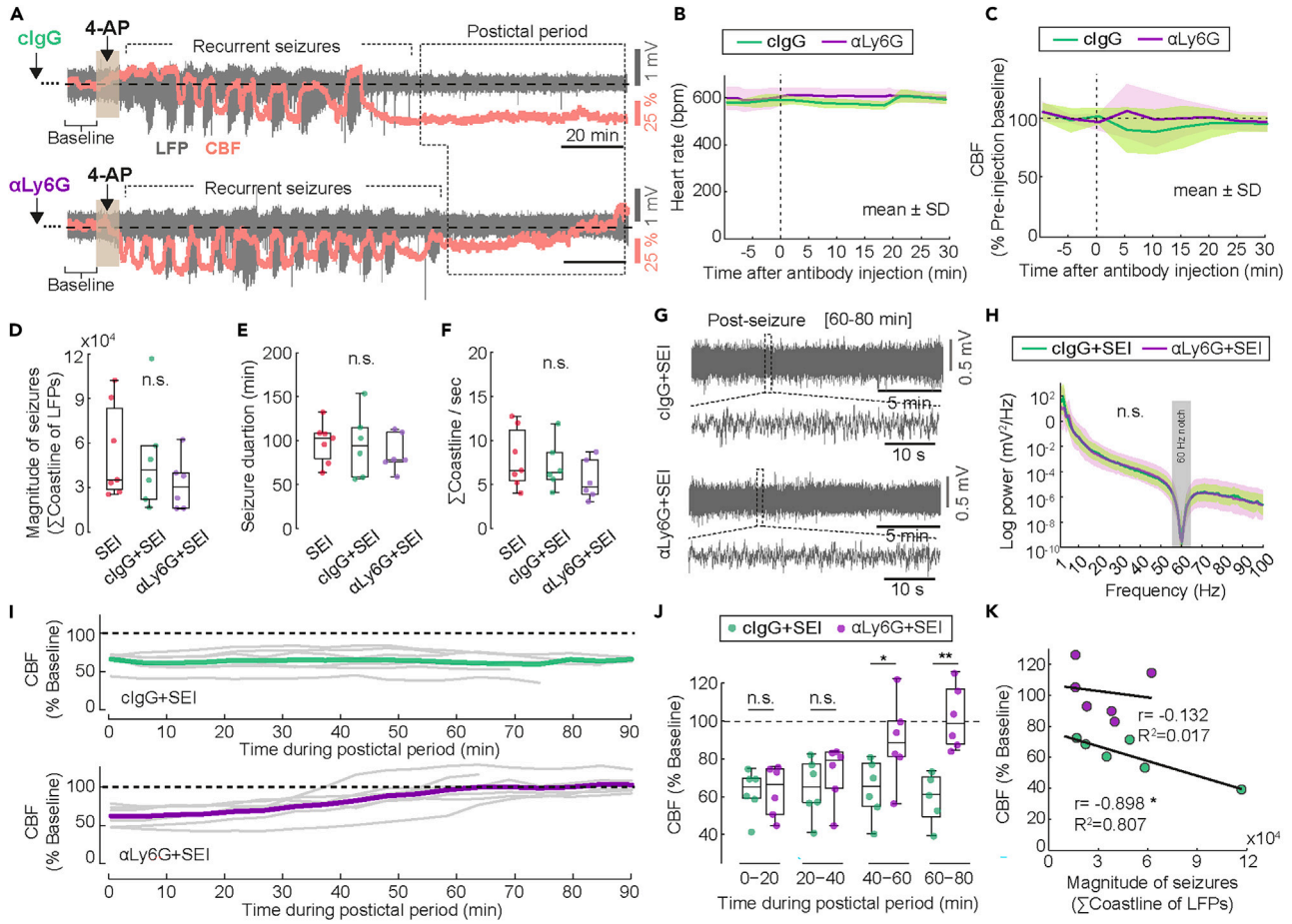

Figure 4. Administration of antibodies against Ly6G ameliorated the postictal CBF reduction

(A) Representative CBF and LFP signals over time with treatment of either isotype control antibody (cIgG) or anti-Ly6G (αLy6G) antibody in 4-AP-injected mice.

(B and C) Time course traces of heart rate and CBF monitored during the antibody injections (cIgG: n = 5; αLy6G: n = 6). CBF signals were normalized to those measured during 10 min before the antibody injections (pre-injection baseline).

(D) Magnitude of recurrent seizures, calculated by summation of coastline lengths of LFP signals (SEI: 53,713.48 ± 29,392.96, n = 7; cIgG+SEI: 49,715.37 ± 33,218.34, n = 6; αLy6G + SEI: 32,587.9 ± 16,306.22, n = 6; $F_{(2,16)}$ = 0.885, p = 0.432, one-way ANOVA test).

(E) Duration of recurrent seizures (SEI: 97.82 ± 21.25, n = 7; cIgG+SEI: 95.24 ± 33.60, n = 6; αLy6G + SEI: 85.58 ± 19.28, n = 6; $F_{(2,16)}$ = 0.344, p = 0.714, one-way ANOVA test).

(F) Averages of summed coastline lengths of LFP signals per second (SEI: 8.73 ± 3.30, n = 7; cIgG+SEI: 7.91 ± 2.53, n = 6; αLy6G + SEI: 6.13 ± 2.23, n = 6; $F_{(2,16)}$ = 1.243, p = 0.315, one-way ANOVA test).

(G) Examples of LFP traces during the 60–80 min of the postictal periods in the cIgG- and αLy6G-treated groups.

(H) Power spectra of LFPs recorded during 60–80 min of the postictal periods (cIgG+SEI, n = 12; αLy6G + SEI, n = 13). "n.s." indicates no statistical significance. Delta (1–4 Hz): $U_{(12,13)}$ = 63, p = 0.415, Mann-Whitney *U* test; theta (4–8 Hz): $t_{(23)}$ = −1.156, p = 0.260, independent *t* test; alpha (8–14 Hz): $U_{(12,13)}$ = 76, p = 0.913, Mann-Whitney *U* test; beta (14–30 Hz): $U_{(12,13)}$ = 77, p = 0.957, Mann-Whitney *U* test; gamma (30–100 Hz): $t_{(20.610)}$ = −0.896, p = 0.380, independent *t* test.

(I) Postictal CBF changes in 4-AP-injected animals that had received isotype control antibody (cIgG+SEI, n = 6) or anti-Ly6G (αLy6G + SEI, n = 6) antibody. The time when the last seizure ended was set "0" to define the beginning of postictal periods in individual mice. The colored lines represent the averaged trace of individual data, which are depicted by the gray lines.

(J) CBF changes in each 20-min epoch of the postictal periods that had received isotype control antibody (cIgG+SEI, n = 6) or anti-Ly6G (αLy6G + SEI, n = 6) antibody. [0–20 min]: 62.65 ± 10.91 (cIgG+SEI) vs. 63.12 ± 12.29 (αLy6G + SEI), $t_{(10)}$ = -0.063, p = 0.951, independent *t* test; [20–40 min]: 64.62 ± 14.18 (cIgG+SEI) vs. 72.44 vs. 14.11 (αLy6G + SEI), $t_{(10)}$ = -0.875, p = 0.402, independent *t* test; [40–60 min]: 64.12 ± 14.01 (cIgG+SEI) vs. 89.57 ± 20.11 (αLy6G + SEI), $t_{(10)}$ = −2.323, *p = 0.043, independent *t* test; [60–80 min]: 59.25 ± 12.23 (cIgG+SEI) vs. 101.87 ± 15.21 (αLy6G + SEI), $t_{(9)}$ = -4.570, **p = 0.001, independent *t* test.

(K) Scatter plots showing the relationship between the magnitude of seizures and the 60–90 min postictal CBF changes in the cIgG- and αLy6G-treated groups (cIgG+SEI: Pearson's *r* = −0.898, *p = 0.015, R^2 = 0.807, n = 6; αLy6G + SEI: Pearson's *r* = −0.132, p = 0.803, R^2 = 0.017, n = 6).

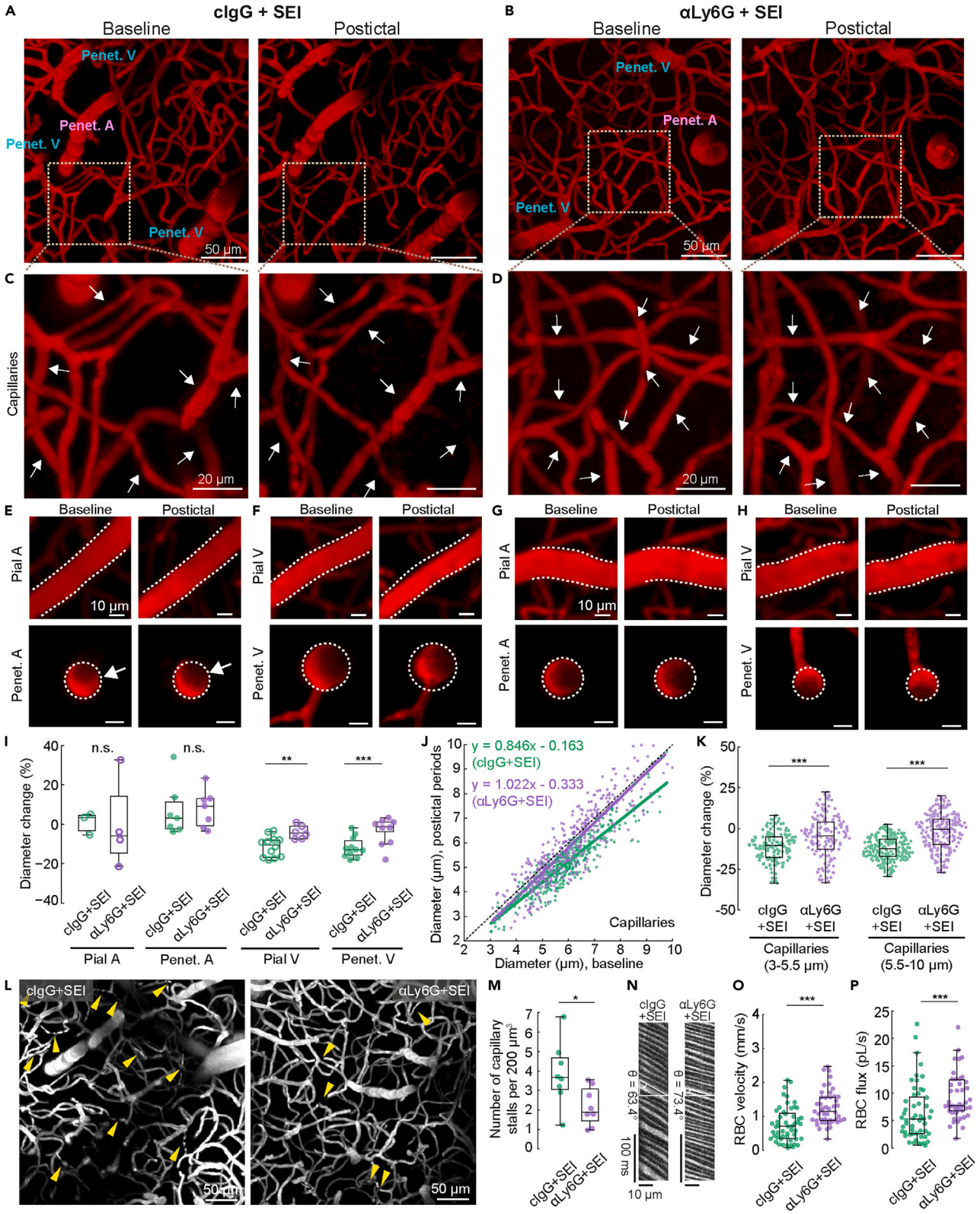
A
cIgG + SEI
Baseline
Postictal
Penet. V
Penet. A
Penet. V
Penet. V
50 μm
B
αLy6G + SEI
Baseline
Postictal
Penet. V
Penet. A
Penet. V
50 μm
C
Capillaries
20 μm
D
20 μm
E
Baseline
Postictal
Pial A
10 μm
Penet. A
F
Baseline
Postictal
Pial V
Penet. V
G
Baseline
Postictal
Pial A
10 μm
Penet. A
H
Baseline
Postictal
Pial V
Penet. V
I
Diameter change (%)
n.s.
n.s.
**
***
cIgG+SEI
αLy6G+SEI
Pial A
Penet. A
Pial V
Penet. V
J
y = 0.846x - 0.163
(cIgG+SEI)
y = 1.022x - 0.333
(αLy6G+SEI)
Capillaries
Diameter (μm), postictal periods
Diameter (μm), baseline
K
Diameter change (%)
***
***
cIgG +SEI
αLy6G +SEI
Capillaries (3-5.5 μm)
Capillaries (5.5-10 μm)
L
cIgG+SEI
αLy6G+SEI
50 μm
50 μm
M
Number of capillary stalls per 200 μm
*
cIgG+SEI
αLy6G+SEI
N
cIgG +SEI
αLy6G +SEI
θ = 63.4°
θ = 73.4°
100 ms
10 μm
O
RBC velocity (mm/s)
***
cIgG+SEI
αLy6G+SEI
P
RBC flux (pL/s)
***
cIgG+SEI
αLy6G+SEI

Figure 5. Effects of administration of the anti-Ly6G antibody on vessel diameter, capillary stalls, and capillary flow of the postictal period

(A and B) Representative two-photon z stack projection images up to ~220 μm excluding the pial surface, obtained during the postictal periods of the cIgG- and αLy6G-treated groups. Penet. A: penetrating arteriole, Penet. V: penetrating venule. Scale bar: 50 μm

(C and D) Magnified images of the areas indicated by dotted squares in (A) and (B), showing capillaries during the postictal periods. Scale bar: 20 μm

(E–H) Examples of pial and penetrating arterioles, and pial and penetrating venules, in baseline and the postictal periods of the cIgG- and αLy6G-treated groups. Scale bar: 10 μm

(I) Pial and penetrating vessel diameter changes (%) during the post periods, compared to the baseline (cIgG+SEI: n = 4, pial arteriole n = 3, penetrating arteriole n = 7, pial venule n = 12, penetrating venule n = 11; αLy6G + SEI: n = 4, pial arteriole n = 4, penetrating arteriole n = 7, pial venule n = 6, penetrating venule n = 9). [Pial A]: 1.01 ± 4.62% (cIgG+SEI) vs. −0.15 ± 20.02% (αLy6G + SEI), $t_{(5)}$ = 0.083, p = 0.937, independent *t* test; [Penet. A]: 7.79 ± 12.42% (cIgG+SEI) vs. 8.89 ± 8.78% (αLy6G + SEI), $U_{(7,7)}$ = 22, p = 0.749, Mann-Whitney *U* test. [Pial V]: −10.89 ± 5.03% (cIgG+SEI) vs. −3.65 ± 3.15% (αLy6G + SEI), $t_{(16)}$ = −3.041, **p = 0.008, independent *t* test; [Penet. V]: −11.55 ± 4.92% (cIgG+SEI) vs. −1.73 ± 4.40% (αLy6G + SEI), $t_{(18)}$ = −4.419, ***p = $3.315e^{-4}$, independent *t* test. "n.s." indicates no statistical significance.

(J) Plot of capillary diameters during baseline versus the postictal periods of the antibody-treated groups (cIgG+SEI: n = 4, vessel segment n = 403; αLy6G + SEI: n = 4, vessel segment n = 399).

(K) Capillary diameter changes (%) in the cIgG- and αLy6G-treated groups during the postictal periods (cIgG+SEI: n = 4; 3–5.5 μm: vessel segment n = 147, 5.5–10 μm: vessel segment n = 256; αLy6G + SEI: n = 4; 3–5.5 μm: vessel segment n = 160, 5.5–10 μm: vessel segment n = 239). [3-5.5 μm]: −11.21 ± 9.26% (cIgG+SEI) vs. −4.69 ± 13.15% (αLy6G + SEI), $t_{(286.172)}$ = −5.041, ***p = $8.233e^{-7}$, independent *t* test; [5.5-10 μm]: −13.15 ± 7.23% (cIgG+SEI) vs. −2.66 ± 10.94% (αLy6G + SEI), $U_{(256,239)}$ = 13,286, ***p = $1.397e^{-27}$, Mann-Whitney *U* test.

(L) Representative two-photon z stack projection images (~100–300 μm below the pial surface) showing capillary segments either stalled (yellow arrowheads) or patent in the two groups.

(M) Quantification of capillary stalling in the cIgG+SEI (n = 8) and the αLy6G + SEI (n = 8) groups. 3.77 ± 1.51 (cIgG+SEI) vs. 2.09 ± 0.91 (αLy6G + SEI), t(14) = 2.520, *p = 0.025, independent t test.

(N) Representative line-scan images acquired in the two groups during the postictal periods.

(O and P) RBC velocity and RBC flux (cIgG+SEI: n = 5, capillary segment n = 53; αLy6G + SEI: n = 5, capillary segments n = 47). [RBC velocity]: 0.76 ± 0.50 (cIgG+SEI) vs. 1.25 ± 0.49 (αLy6G + SEI), U(53,47) = 585, ***p = 5.077e-6, Mann-Whitney U test; [RBC flux]: 6.40 ± 5.05 (cIgG+SEI) vs. 9.89 ± 5.21 (αLy6G + SEI), U(53,47) = 703, ***p = 1.792e-4, Mann-Whitney U test.

diameters at baseline and during the postictal period were similar (Figures 5E, 5G, and 5I; see also Figure S8A) aforementioned. The postictal capillary diameters compared to baseline remained reduced in the isotype group, whereas the reductions were alleviated in the anti-Ly6G group (Figures 5C, 5D, 5J, and 5K). The postictal venule diameters also recovered in the anti-Ly6G group, but not in the control isotype group (Figures 5F, 5H, and 5I; see also Figure S8B). Capillary stalling (Figures 5L and 5M), and the number of neutrophil plugs were apparently decreased (Figures S8C and S8D). Moreover, RBC flow and flux measured in capillaries were significantly increased in the anti-Ly6G group (Figures 5N–5P). These results imply that increased capillary stalling induced by neutrophil plugs were the main cause of prolonged CBF reductions, which were associated with reduced capillary and venule diameter

Elevated expression of ICAM-1 proteins and administration of an antibody targeting LFA-1

We next sought to examine the underlying molecular changes that led to increased neutrophil plugging in capillaries. The adhesion of leukocytes, including neutrophils, to the vascular endothelium is mediated by leukocyte-binding receptors expressed on the endothelial cell surface, such as P- and E-selectin, ICAM-1 and VCAM-1.[30,46,47] We surmised that increased expression of these factors may mediate increased neutrophil adhesion, thus resulting in neutrophil plugging and increased capillary stalling. We analyzed the expression level of selectins and adhesion molecules relative to GAPDH protein in brain tissue obtained from control and postictal mice with an immunoblotting assay (Figure 6A). Among the four types of vascular adhesion molecules, only ICAM-1 showed increased protein expression in the postictal mouse brains (Figure 6B). ICAM-1 can mediate neutrophil adhesion via interaction with LFA-1, which is an integrin receptor expressed on neutrophils.[48–50] From these results, we hypothesized that the increased neutrophil plugging was mediated by increased interactions between LFA-1 and ICAM-1. We then tested whether the administration of antibodies targeting to LFA-1 can alleviate the persistent CBF reductions observed during the postictal period. The anti-LFA-1 antibody was also administered 40 min before the 4-AP injection (Figure 6C) in the same manner described for the anti-Ly6G group. The anti-LFA-1 group showed a similar magnitude and duration of seizures (Figure S9) compared to those observed in the other groups (Figures 4D–4F). The anti-LFA-1 antibody induced no apparent changes in physiological conditions or baseline CBF levels (Figure 6D). Notably, the anti-LFA-1-treated group showed a gradual recovery of CBF during the postictal period (Figure 6E). The decreased CBF was significantly increased within 40–60 min (Figure 6F), as shown in the anti-Ly6G group (Figures 4I and 4J). The dynamics of the postictal CBF for each 20-min epoch were similar to those observed in the anti-Ly6G group. Taken together, these results show that neutrophil adhesion to brain capillaries may increase via binding of LFA-1 to ICAM-1, thus leading to a prolonged decrease in CBF.

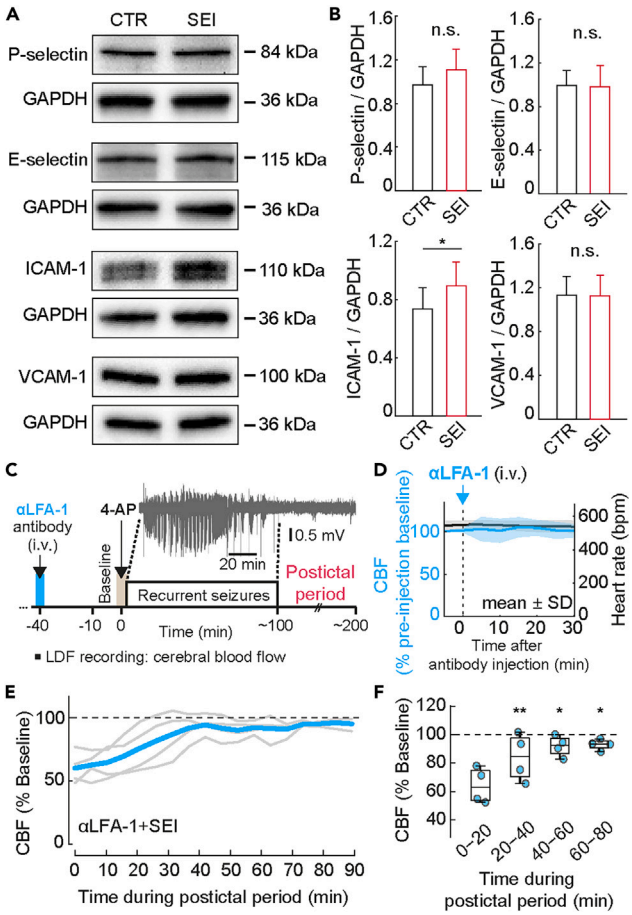

Figure 6. Protein expression level of endothelial adhesion molecules

(A) Western blot bands of P-selectin, E-selectin, ICAM-1, and VCAM-1 with each control protein (GAPDH) from the control (CTR) and the postictal (SEI) animals.

(B) Quantification of blots as the ratio of P-selectin, E-selectin, ICAM-1 and VCAM-1 expression levels, normalized to the corresponding GAPDH levels. Data are represented as mean ± SD (CTR: n = 9; SEI: n = 9). [P-selectin]: 0.97 ± 0.16 (CTR) vs. 1.11 ± 0.18 (SEI), $U_{(9,9)}$ = 26, p = 0.2, Mann-Whitney *U* test; [E-selectin]: 0.99 ± 0.14 (CTR) vs. 0.98 ± 0.19 (SEI), $U_{(9,9)}$ = 38, p = 0.825, Mann-Whitney *U* test; [ICAM-1]: 0.73 ± 0.14 (CTR) vs. 0.89 ± 0.16 (SEI), $U_{(9,9)}$ = 17, *p = 0.038, Mann-Whitney *U* test; [VCAM-1]: 1.13 ± 0.17 (CTR) vs. 1.13 ± 0.19 (SEI), $U_{(9,9)}$ = 29, p = 0.310, Mann-Whitney *U* test. "n.s." indicates no statistical significance.

(C) Schematic representation of the experimental procedures for administration of the anti-LFA-1 (αLFA-1) antibody.

(D) Time course traces of heart rate and CBF monitored before and after the anti-LFA-1 antibody injection.

(E) CBF changes during the postictal period of 4-AP-injected animals that had received the anti-LFA-1 (αLFA-1) antibody (αLFA-1+SEI: n = 4). The colored lines represent the averaged trace of individual data, which are depicted by the gray lines.

(F) CBF changes in each 20-min epoch of the postictal periods in the αLFA-1+SEI group (n = 4, 0–20 min: 64.23 ± 10.83, 20–40 min: 84.06 ± 14.29, 40–60 min: 92.00 ± 6.35, 60–80 min: 93.04 ± 3.25, $F(3,9)$ = 14.894, p = 0.001, one-way repeated ANOVA test, 0–20 min vs. 20–40 min: **p = 0.007, 0–20 min vs. 40–60 min: *p = 0.012, 0–20 min vs. 60–80 min: *p = 0.010 by Bonferroni *post hoc* comparisons.

DISCUSSION

The differential contribution of arterial and capillary changes to the postictal hypoperfusion

In our study, postictal hypoperfusion was observed in combination with vascular changes in different vessel compartments, including arteriolar constriction and capillary stalling. Arteriolar constriction was observed immediately after the offset of seizures, and it was sustained until 20–30 min into the postictal period. This is consistent with a report showing that arteriolar constriction resulted in postictal hypoperfusion following a brief seizure event induced in an electrical kindling model.[24] Arteriolar diameters gradually recovered to baseline levels thereafter. However, the CBF decrease was observed to persist for more than an hour.

When the anti-Ly6G antibody was administered, the return of arteriole diameters to the baseline values was not changed and was similar to the dynamics of CBF recovery during the postictal period. Considering that the anti-Ly6G antibody resolved only the prolonged hypoperfusion, arterial constriction during the early phase was independent of neutrophil adhesion, while the later long-lasting CBF reduction was due to capillary stalling induced by neutrophil plugs. This condition was also accompanied by capillary and venous constriction. We propose that vascular changes in different vessel compartments can differentially contribute to hypoperfusion in a time-dependent manner.

Our results show that reducing the incidence of neutrophil plugging in capillary segments via the anti-Ly6G antibody treatment could prevent the long-lasting decrease in postictal CBF, implying that it can be the main cause of sustained hypoperfusion. Our observation is consistent with other studies showing that neutrophil plugging had a significant impact on cortical hypoperfusion in AD and ischemic stroke mouse models.[41,42] Hernandez et al.[42] also reported that 1.8% of stalled capillaries led to 17% decrease in CBF in simulated vascular networks, indicating that stalling in even a small proportion of capillaries can have a significant impact on CBF.

We also observed capillary constrictions during the postictal period. This change may be related to neutrophil adhesion that causes capillary stalling. Cruz Hernandez et al.[42] also reported that stalled capillaries had a lower average diameter than flowing capillaries in AD mouse brains. Moreover, increased adhesive interactions between neutrophils and endothelial cells result in the augmented production of cytotoxic agents such as reactive oxygen species (ROS) and proteases.[51–54] Seizure activity can induce these conditions due to increased production of proinflammatory cytokines that activate vascular endothelial cells to express leukocyte-binding adhesion molecules.[29] These can cause microvascular injury and vascular dysfunction in epilepsy,[55–57] which might be reflected by capillary and venous constriction in our results. A decreased volume flux through capillaries was also observed in our results, which might contribute to the reduced venous diameters. Capillary and venous constriction may aggravate impaired microcirculation, contributing to the prolonged hypoperfusion.

The underlying mechanism of increased neutrophil adhesion during the postictal period

Our results showed that the anti-Ly6G antibody could prevent neutrophil plugging in the postictal mouse brain. The observation time point for the postictal period was 3–4 h after the antibody injection, which was not a sufficient time to change the number of neutrophils in the blood,[42,43] implying that the effect observed in this study was not due to neutrophil depletion. One to 2 h was sufficient for the antibody injection to resolve capillary stalling in AD and ischemic stroke animal models,[42,43] also suggesting that reduced neutrophil counts may not be necessary for this effect. We consider that the antibody may inhibit receptor-mediated adhesive interactions of neutrophils with the vascular endothelium. Our data revealed that ICAM-1 expression was specifically elevated in the postictal mouse brains and that the prolonged CBF reductions were also recovered by an antibody targeting LFA-1 that mediates neutrophil adhesion to ICAM-1.[49,50] The temporal characteristics of CBF recovery in the anti-LFA-1 antibody group were similar to those in the anti-Ly6G antibody group, implying that these two antibodies may share a similar mechanism to prevent neutrophil adhesion and plugging in brain microvessels. Wang et al.[58] also reported that Ly6G ligation was related to the attenuation of β2-integrin-dependent adhesion, which is one of the key integrins that mediate leukocyte adhesion to the vascular endothelium.[59] β2-integrin is one of the two subunits that comprise LFA-1.[60] Taken together, our findings suggest that the increased neutrophil plugging might be result from increased adhesive interactions between neutrophils and brain capillaries via LFA-1 and increased ICAM-1 expression.

Other studies also reported that epileptiform activities induced endothelial expression of leukocyte adhesion molecules, including ICAM-1, VCAM-1, and P-selectin.[28,29] The observation time for these adhesion molecules was 5–6 h after epileptiform activities, while ours was up to 1–2 h. Our finding may imply that ICAM-1 expression initially increases in the postictal state, thus playing a key role in a series of vascular inflammatory responses in the postictal brain. The expression of other leukocyte adhesion molecules, such as VCAM-1 and P-selectin,[28,29] may increase later, exacerbating stalled blood flow during chronic periods. Further study is required to examine cerebral perfusion changes with differential expression of adhesion molecules and how these changes contribute to the development of pathology and neurological function in chronic epilepsy.

Clinical relevance

Abnormal brain blood flow and metabolic changes have long been reported in epilepsy patients.[61–63] Hypoperfusion has not only been used as a biomarkers to localize an epileptogenic focus but also been proposed as an important factor underlying the pathophysiology of epilepsy.[4,24] For instance, oxidative stress caused by a prolonged CBF decrease can aggravate cellular damage induced by epileptic seizures. A recent animal study also showed that postictal hypoperfusion leads to hypoxic conditions in the brain, thus resulting in behavioral impairments such as memory loss.[24] Leal-campanario et al.[64] showed that the distribution of apoptotic cells was associated with the site of disturbed capillary blood flow in epileptic mouse brains. Given the central role of cellular damage in epileptogenesis,[65] preventing damaging effects of prolonged hypoperfusion could be helpful for the treatment of epilepsy.

It was reported that the number of neutrophils is increased in postictal human blood samples,[66–68] which might be linked to increased neutrophil plugging in cerebral vessels. This condition can negatively affect the brain cells, leading to neurological dysfunction, and exacerbating the pathology of chronic epilepsy. We suggest that preventing capillary stalling by inhibiting neutrophil adhesion may be a preventative treatment for epilepsy. This effect might be achieved by blockade of a receptor-mediated interaction of neutrophils with the vascular endothelium. Moreover, the therapeutic approach might be applicable for other brain diseases that are accompanied by chronic brain inflammation with vascular dysfunction and chronic hypoperfusion.

Limitations of the study

The acute model used in this study was characterized by intermittent and recurrent seizures that lasted for ~1.6 h. The findings presented in this study would not be applicable to all cases of postictal state, such as those following a single brief seizure that is not intense enough to induce the increased neutrophil adhesion. However, postictal duration were variable from a few minutes to a few hours in epilepsy patients experiencing a single event of generalized seizure,[69] and inflammatory responses measured by cytokine levels were varied after a single seizure.[70–72] We believe that our findings shown have important implications not only for the postictal brain after a prolonged seizure but also for cases of chronic seizures that occur in brains vulnerable to inflammatory changes. Further investigation is also required to examine whether prevention of neutrophil adhesion induced by upcoming seizures would be beneficial during a chronic epileptic condition with intermittent seizures. Neutrophil adhesion that may accumulate during chronic seizures could exacerbate the prolonged hypoperfusion and other seizure-related damaging effects. Additionally, ICAM-1 is not only expressed in endothelial cells but also in microglia and astrocyte in pathological states in the brain.[73] The increased protein expression of ICAM-1 presented in our study may also include its expression in these cell types, as the endothelial cells were not separately isolated from the brain samples during the western blot analysis.

STAR★METHODS

Detailed methods are provided in the online version of this paper and include the following:

- KEY RESOURCES TABLE
- RESOURCE AVAILABILITY
  - Lead contact
  - Materials availability
  - Data and code availability
- EXPERIMENTAL MODEL AND SUBJECT DETAILS
  - Animals
  - Experimental design
- METHOD DETAILS
  - Animal preparation
  - Seizure model establishment and electrophysiology
  - CBF recording by laser Doppler flowmetry (LDF)
  - Two-photon vasculature imaging
  - RBC velocity
  - Neutrophil staining and confocal microscopy imaging
  - Antibody treatment
  - Western blotting

- QUANTIFICATION AND STATISTICAL ANALYSIS
  - CBF change
  - Vessel diameter
  - Quantification of flowing and nonflowing vessel segments
  - RBC velocity and flux
  - LFP data
  - Statistics

SUPPLEMENTAL INFORMATION

Supplemental information can be found online at https://doi.org/10.1016/j.isci.2023.106655.

ACKNOWLEDGMENTS

This work was supported by the Institute for Basic Science (No. IBS-R015-D1); the National Research Foundation of Korea (NRF) funded by the Korea government (MSIT) (No. 2017R1A6A1A03015642, 2023R1A2C1004318); Basic Science Research Program through the NRF funded by the Ministry of Education (No. 2021R1I1A1A01059610, 2021R1I1A1A01057989); the Fourth Stage of Brain Korea 21 Project in Department of Intelligent Precision Healthcare, Sungkyunkwan University (SKKU) (No. S-2022-0608-000); Institute of Information & Communications Technology Planning & Evaluation (IITP) funded by the Korea government (MSIT) (No. 20200002610011001). This research was also supported by IMNEWRUN Inc.

AUTHOR CONTRIBUTIONS

H.-K.L. and M.S. conceived and designed the experiments. H.-K.L. carried out all *in vivo* two-photon imaging experiments and histology studies. S.B. performed the laser Doppler flowmetry experiments. K.H. performed western blotting experiments. H.-K.L., S.B., K.H., and B.-M.K. performed data analysis. Y.J. contributed to preparation for two-photon imaging experiments and histology studies. H.-K.L. and M.S. interpreted results and wrote the manuscript. S.-G.K. provided expertise and reviewed the manuscript. All authors reviewed and approved the final manuscript.

DECLARATION OF INTERESTS

The authors declare no competing interests.

Received: December 18, 2022
Revised: March 23, 2023
Accepted: April 6, 2023
Published: April 10, 2023

REFERENCES

1. Iadecola, C. (2004). Neurovascular regulation in the normal brain and in Alzheimer's disease. Nat. Rev. Neurosci. *5*, 347–360. https://doi.org/10.1038/nrn1387.

2. Iadecola, C. (2013). The pathobiology of vascular dementia. Neuron *80*, 844–866. https://doi.org/10.1016/j.neuron.2013.10.008.

3. Sweeney, M.D., Kisler, K., Montagne, A., Toga, A.W., and Zlokovic, B.V. (2018). The role of brain vasculature in neurodegenerative disorders. Nat. Neurosci. *21*, 1318–1331. https://doi.org/10.1038/s41593-018-0234-x.

4. Farrell, J.S., Colangeli, R., Wolff, M.D., Wall, A.K., Phillips, T.J., George, A., Federico, P., and Teskey, G.C. (2017). Postictal hypoperfusion/hypoxia provides the foundation for a unified theory of seizure-induced brain abnormalities and behavioral dysfunction. Epilepsia *58*, 1493–1501. https://doi.org/10.1111/epi.13827.

5. Borghammer, P., Chakravarty, M., Jonsdottir, K.Y., Sato, N., Matsuda, H., Ito, K., Arahata, Y., Kato, T., and Gjedde, A. (2010). Cortical hypometabolism and hypoperfusion in Parkinson's disease is extensive: probably even at early disease stages. Brain Struct. Funct. *214*, 303–317. https://doi.org/10.1007/s00429-010-0246-0.

6. Wolters, F.J., Zonneveld, H.I., Hofman, A., van der Lugt, A., Koudstaal, P.J., Vernooij, M.W., and Ikram, M.A.; Heart-Brain Connection Collaborative Research Group (2017). Cerebral perfusion and the risk of dementia: a population-based study. Circulation *136*, 719–728. https://doi.org/10.1161/CIRCULATIONAHA.117.027448.

7. D'Haeseleer, M., Hostenbach, S., Peeters, I., Sankari, S.E., Nagels, G., De Keyser, J., and D'hooghe, M.B. (2015). Cerebral hypoperfusion: a new pathophysiologic concept in multiple sclerosis? J. Cerebr. Blood Flow Metabol. *35*, 1406–1410. https://doi.org/10.1038/jcbfm.2015.131.

8. Dong, S., Maniar, S., Manole, M.D., and Sun, D. (2018). Cerebral hypoperfusion and other shared brain pathologies in ischemic stroke and Alzheimer's disease. Transl. Stroke Res. *9*, 238–250. https://doi.org/10.1007/s12975-017-0570-2.

9. Wong, S.M., Jansen, J.F.A., Zhang, C.E., Hoff, E.I., Staals, J., van Oostenbrugge, R.J., and Backes, W.H. (2019). Blood-brain barrier impairment and hypoperfusion are linked in cerebral small vessel disease. Neurology *92*, e1669–e1677. https://doi.org/10.1212/WNL.0000000000007263.

10. Farrell, J.S., Gaxiola-Valdez, I., Wolff, M.D., David, L.S., Dika, H.I., Geeraert, B.L., Rachel Wang, X., Singh, S., Spanswick, S.C., Dunn, J.F., et al. (2016). Postictal behavioural impairments are due to a severe prolonged hypoperfusion/hypoxia event that is COX-2 dependent. Elife *5*, e19352. https://doi.org/10.7554/eLife.19352.

11. Gaxiola-Valdez, I., Singh, S., Perera, T., Sandy, S., Li, E., and Federico, P. (2017). Seizure onset zone localization using postictal hypoperfusion detected by arterial spin labelling MRI. Brain *140*, 2895–2911. https://doi.org/10.1093/brain/awx241.

12. Pizzini, F.B., Farace, P., Manganotti, P., Zoccatelli, G., Bongiovanni, L.G., Golay, X., Beltramello, A., Osculati, A., Bertini, G., and Fabene, P.F. (2013). Cerebral perfusion alterations in epileptic patients during peri-ictal and post-ictal phase: PASL vs DSC-MRI. Magn. Reson. Imaging *31*, 1001–1005. https://doi.org/10.1016/j.mri.2013.03.023.

13. Weinand, M.E., Carter, L.P., Patton, D.D., Oommen, K.J., Labiner, D.M., and Talwar, D. (1994). Long-term surface cortical cerebral blood flow monitoring in temporal lobe epilepsy. Neurosurgery *35*, 657–664. https://doi.org/10.1227/00006123-199410000-00011.

14. Leonhardt, G., de Greiff, A., Weber, J., Ludwig, T., Wiedemayer, H., Forsting, M., and Hufnagel, A. (2005). Brain perfusion following single seizures. Epilepsia *46*, 1943–1949. https://doi.org/10.1111/j.1528-1167.2005.00336.x.

15. Josephson, C.B., Engbers, J.D.T., Sajobi, T.T., Jette, N., Agha-Khani, Y., Federico, P., Murphy, W., Pillay, N., and Wiebe, S. (2016). An investigation into the psychosocial effects of the postictal state. Neurology *86*, 723–730. https://doi.org/10.1212/WNL.0000000000002398.

16. Fisher, R.S., and Schachter, S.C. (2000). The postictal state: a neglected entity in the management of epilepsy. Epilepsy Behav. *1*, 52–59. https://doi.org/10.1006/ebeh.2000.0023.

17. Berg, A.T. (2011). Epilepsy, cognition, and behavior: the clinical picture. Epilepsia *52*, 7–12. https://doi.org/10.1111/j.1528-1167.2010.02905.x.

18. Pottkämper, J.C.M., Hofmeijer, J., van Waarde, J.A., and van Putten, M.J.A.M. (2020). The postictal state - what do we know? Epilepsia *61*, 1045–1061. https://doi.org/10.1111/epi.16519.

19. Kaibara, M., and Blume, W.T. (1988). The postictal electroencephalogram. Electroencephalogr. Clin. Neurophysiol. *70*, 99–104. https://doi.org/10.1016/0013-4694(88)90109-5.

20. So, N.K., and Blume, W.T. (2010). The postictal EEG. Epilepsy Behav. *19*, 121–126. https://doi.org/10.1016/j.yebeh.2010.06.033.

21. Yarnell, P.R. (1975). Todd's paralysis: a cerebrovascular phenomenon? Stroke *6*, 301–303. https://doi.org/10.1161/01.str.6.3.301.

22. Mathews, M.S., Smith, W.S., Wintermark, M., Dillon, W.P., and Binder, D.K. (2008). Local cortical hypoperfusion imaged with CT perfusion during postictal Todd's paresis. Neuroradiology *50*, 397–401. https://doi.org/10.1007/s00234-008-0362-1.

23. Masterson, K., Vargas, M.I., and Delavelle, J. (2009). Postictal deficit mimicking stroke: role of perfusion CT. J. Neuroradiol. *36*, 48–51. https://doi.org/10.1016/j.neurad.2008.08.006.

24. Farrell, J.S., Colangeli, R., Dudok, B., Wolff, M.D., Nguyen, S.L., Jackson, J., Dickson, C.T., Soltesz, I., and Teskey, G.C. (2020). In vivo assessment of mechanisms underlying the neurovascular basis of postictal amnesia. Sci. Rep. *10*, 14992. https://doi.org/10.1038/s41598-020-71935-6.

25. Vezzani, A., and Granata, T. (2005). Brain inflammation in epilepsy: experimental and clinical evidence. Epilepsia *46*, 1724–1743. https://doi.org/10.1111/j.1528-1167.2005.00298.x.

26. Vezzani, A., French, J., Bartfai, T., and Baram, T.Z. (2011). The role of inflammation in epilepsy. Nat. Rev. Neurol. *7*, 31–40. https://doi.org/10.1038/nrneurol.2010.178.

27. Li, G., Bauer, S., Nowak, M., Norwood, B., Tackenberg, B., Rosenow, F., Knake, S., Oertel, W.H., and Hamer, H.M. (2011). Cytokines and epilepsy. Seizure *20*, 249–256. https://doi.org/10.1016/j.seizure.2010.12.005.

28. Librizzi, L., Regondi, M.C., Pastori, C., Frigerio, S., Frassoni, C., and de Curtis, M. (2007). Expression of adhesion factors induced by epileptiform activity in the endothelium of the isolated Guinea pig brain in vitro. Epilepsia *48*, 743–751. https://doi.org/10.1111/j.1528-1167.2007.01047.x.

29. Fabene, P.F., Navarro Mora, G., Martinello, M., Rossi, B., Merigo, F., Ottoboni, L., Bach, S., Angiari, S., Benati, D., Chakir, A., et al. (2008). A role for leukocyte-endothelial adhesion mechanisms in epilepsy. Nat. Med. *14*, 1377–1383. https://doi.org/10.1038/nm.1878.

30. Phillipson, M., and Kubes, P. (2011). The neutrophil in vascular inflammation. Nat. Med. *17*, 1381–1390. https://doi.org/10.1038/nm.2514.

31. Greenwood, J., Heasman, S.J., Alvarez, J.I., Prat, A., Lyck, R., and Engelhardt, B. (2011). Review: leucocyte-endothelial cell crosstalk at the blood-brain barrier: a prerequisite for successful immune cell entry to the brain. Neuropathol. Appl. Neurobiol. *37*, 24–39. https://doi.org/10.1111/j.1365-2990.2010.01140.x.

32. Takeshita, Y., and Ransohoff, R.M. (2012). Inflammatory cell trafficking across the blood-brain barrier: chemokine regulation and in vitro models. Immunol. Rev. *248*, 228–239. https://doi.org/10.1111/j.1600-065X.2012.01127.x.

33. Yu, X., Ji, C., and Shao, A. (2020). Neurovascular unit dysfunction and neurodegenerative disorders. Front. Neurosci. *14*, 334. https://doi.org/10.3389/fnins.2020.00334.

34. Stanimirovic, D.B., and Friedman, A. (2012). Pathophysiology of the neurovascular unit: disease cause or consequence? J. Cerebr. Blood Flow Metabol. *32*, 1207–1221. https://doi.org/10.1038/jcbfm.2012.25.

35. Guo, X., and Zhao, Z. (2022). Vascular inflammation in the central nervous system. Neural Regen. Res. *17*, 1728–1730. https://doi.org/10.4103/1673-5374.332140.

36. Lim, H.K., You, N., Bae, S., Kang, B.M., Shon, Y.M., Kim, S.G., and Suh, M. (2021). Differential contribution of excitatory and inhibitory neurons in shaping neurovascular coupling in different epileptic neural states. J. Cerebr. Blood Flow Metabol. *41*, 1145–1161. https://doi.org/10.1177/0271678X20934071.

37. White, A.M., Williams, P.A., Ferraro, D.J., Clark, S., Kadam, S.D., Dudek, F.E., and Staley, K.J. (2006). Efficient unsupervised algorithms for the detection of seizures in continuous EEG recordings from rats after brain injury. J. Neurosci. Methods *152*, 255–266. https://doi.org/10.1016/j.jneumeth.2005.09.014.

38. Niknazar, M., Mousavi, S.R., Motaghi, S., Dehghani, A., Vosoughi Vahdat, B., Shamsollahi, M.B., Sayyah, M., and Noorbakhsh, S.M. (2013). A unified approach for detection of induced epileptic seizures in rats using ECoG signals. Epilepsy Behav. *27*, 355–364. https://doi.org/10.1016/j.yebeh.2013.01.028.

39. Grant, R.I., Hartmann, D.A., Underly, R.G., Berthiaume, A.A., Bhat, N.R., and Shih, A.Y. (2019). Organizational hierarchy and structural diversity of microvascular pericytes in adult mouse cortex. J. Cerebr. Blood Flow Metabol. *39*, 411–425. https://doi.org/10.1177/0271678X17732229.

40. Ali, M., Falkenhain, K., Njiru, B.N., Murtaza-Ali, M., Ruiz-Uribe, N.E., Haft-Javaherian, M., Catchers, S., Nishimura, N., Schaffer, C.B., and Bracko, O. (2022). VEGF signalling causes stalls in brain capillaries and reduces cerebral blood flow in Alzheimer's mice. Brain *145*, 1449–1463. https://doi.org/10.1093/brain/awab387.

41. El Amki, M., Glück, C., Binder, N., Middleham, W., Wyss, M.T., Weiss, T., Meister, H., Luft, A., Weller, M., Weber, B., and Wegener, S. (2020). Neutrophils obstructing brain capillaries are a major cause of No-reflow in ischemic stroke. Cell Rep. *33*, 108260. https://doi.org/10.1016/j.celrep.2020.108260.

42. Cruz Hernández, J.C., Bracko, O., Kersbergen, C.J., Muse, V., Haft-Javaherian, M., Berg, M., Park, L., Vinarcsik, L.K., Ivasyk, I., Rivera, D.A., et al. (2019). Neutrophil adhesion in brain capillaries reduces cortical blood flow and impairs memory function in Alzheimer's disease mouse models. Nat. Neurosci. *22*, 413–420. https://doi.org/10.1038/s41593-018-0329-4.

43. Erdener, Ş.E., Tang, J., Kılıç, K., Postnov, D., Giblin, J.T., Kura, S., Chen, I.C.A., Vayisoğlu, T., Sakadžić, S., Schaffer, C.B., and Boas, D.A. (2021). Dynamic capillary stalls in reperfused ischemic penumbra contribute to injury: a hyperacute role for neutrophils in persistent traffic jams. J. Cerebr. Blood Flow Metabol. *41*, 236–252. https://doi.org/10.1177/0271678X20914179.

44. Baik, S.H., Cha, M.Y., Hyun, Y.M., Cho, H., Hamza, B., Kim, D.K., Han, S.H., Choi, H., Kim, K.H., Moon, M., et al. (2014). Migration of neutrophils targeting amyloid plaques in Alzheimer's disease mouse model. Neurobiol. Aging *35*, 1286–1292. https://doi.org/10.1016/j.neurobiolaging.2014.01.003.

45. Daley, J.M., Thomay, A.A., Connolly, M.D., Reichner, J.S., and Albina, J.E. (2008). Use of Ly6G-specific monoclonal antibody to deplete neutrophils in mice. J. Leukoc. Biol. *83*, 64–70. https://doi.org/10.1189/jlb.0407247.

46. Gauberti, M., Fournier, A.P., Docagne, F., Vivien, D., and Martinez de Lizarrondo, S. (2018). Molecular magnetic resonance imaging of endothelial activation in the central nervous system. Theranostics *8*, 1195–1212. https://doi.org/10.7150/thno.22662.

47. Rossi, B., Angiari, S., Zenaro, E., Budui, S.L., and Constantin, G. (2011). Vascular inflammation in central nervous system diseases: adhesion receptors controlling leukocyte-endothelial interactions. J. Leukoc. Biol. *89*, 539–556. https://doi.org/10.1189/jlb.0710432.

48. Marlin, S.D., and Springer, T.A. (1987). Purified intercellular adhesion molecule-1 (ICAM-1) is a ligand for lymphocyte function-associated antigen 1 (LFA-1). Cell *51*, 813–819. https://doi.org/10.1016/0092-8674(87)90104-8.

49. Ding, Z.M., Babensee, J.E., Simon, S.I., Lu, H., Perrard, J.L., Bullard, D.C., Dai, X.Y., Bromley, S.K., Dustin, M.L., Entman, M.L., et al. (1999). Relative contribution of LFA-1 and Mac-1 to neutrophil adhesion and migration. J. Immunol. *163*, 5029–5038.

50. Henderson, R.B., Lim, L.H., Tessier, P.A., Gavins, F.N., Mathies, M., Perretti, M., and Hogg, N. (2001). The use of lymphocyte function-associated antigen (LFA)-1-deficient mice to determine the role of LFA-1, Mac-1, and alpha4 integrin in the inflammatory response of neutrophils. J. Exp. Med. *194*, 219–226. https://doi.org/10.1084/jem.194.2.219.

51. Domínguez-Luis, M.J., Armas-González, E., Herrera-García, A., Arce-Franco, M., Feria, M., Vicente-Manzanares, M., Martínez-Ruiz, A., Sánchez-Madrid, F., and Díaz-González, F. (2019). L-selectin expression is regulated by CXCL8-induced reactive oxygen species produced during human neutrophil rolling. Eur. J. Immunol. *49*, 386–397. https://doi.org/10.1002/eji.201847710.

52. Meegan, J.E., Yang, X., Coleman, D.C., Jannaway, M., and Yuan, S.Y. (2017). Neutrophil-mediated vascular barrier injury: role of neutrophil extracellular traps. Microcirculation *24*, e12352. https://doi.org/10.1111/micc.12352.

53. Yuan, S.Y., Shen, Q., Rigor, R.R., and Wu, M.H. (2012). Neutrophil transmigration, focal adhesion kinase and endothelial barrier function. Microvasc. Res. *83*, 82–88. https://doi.org/10.1016/j.mvr.2011.06.015.

54. Smyth, L.C.D., Murray, H.C., Hill, M., van Leeuwen, E., Highet, B., Magon, N.J., Osanlouy, M., Mathiesen, S.N., Mockett, B., Singh-Bains, M.K., et al. (2022). Neutrophil-vascular interactions drive myeloperoxidase accumulation in the brain in Alzheimer's disease. Acta Neuropathol. Commun. *10*, 38. https://doi.org/10.1186/s40478-022-01347-2.

55. Parfenova, H., Carratu, P., Tcheranova, D., Fedinec, A., Pourcyrous, M., and Leffler, C.W. (2005). Epileptic seizures cause extended postictal cerebral vascular dysfunction that is prevented by HO-1 overexpression. Am. J. Physiol. Heart Circ. Physiol. *288*, H2843–H2850. https://doi.org/10.1152/ajpheart.01274.2004.

56. Zimmermann, A., Leffler, C.W., Tcheranova, D., Fedinec, A.L., and Parfenova, H. (2007). Cerebroprotective effects of the CO-releasing molecule CORM-A1 against seizure-induced neonatal vascular injury. Am. J. Physiol. Heart Circ. Physiol. *293*, H2501–H2507. https://doi.org/10.1152/ajpheart.00354.2007.

57. Prager, O., Kamintsky, L., Hasam-Henderson, L.A., Schoknecht, K., Wuntke, V., Papageorgiou, I., Swolinsky, J., Muoio, V., Bar-Klein, G., Vazana, U., et al. (2019). Seizure-induced microvascular injury is associated with impaired neurovascular coupling and blood-brain barrier dysfunction. Epilepsia *60*, 322–336. https://doi.org/10.1111/epi.14631.

58. Wang, J.X., Bair, A.M., King, S.L., Shnayder, R., Huang, Y.F., Shieh, C.C., Soberman, R.J., Fuhlbrigge, R.C., and Nigrovic, P.A. (2012). Ly6G ligation blocks recruitment of neutrophils via a beta2-integrin-dependent mechanism. Blood *120*, 1489–1498. https://doi.org/10.1182/blood-2012-01-404046.

59. Fagerholm, S.C., Guenther, C., Llort Asens, M., Savinko, T., and Uotila, L.M. (2019). Beta2-Integrins and interacting proteins in leukocyte trafficking, immune suppression, and immunodeficiency disease. Front. Immunol. *10*, 254. https://doi.org/10.3389/fimmu.2019.00254.

60. Kourtzelis, I., Mitroulis, I., von Renesse, J., Hajishengallis, G., and Chavakis, T. (2017). From leukocyte recruitment to resolution of inflammation: the cardinal role of integrins. J. Leukoc. Biol. *102*, 677–683. https://doi.org/10.1189/jlb.3MR0117-024R.

61. Van Paesschen, W., Dupont, P., Sunaert, S., Goffin, K., and Van Laere, K. (2007). The use of SPECT and PET in routine clinical practice in epilepsy. Curr. Opin. Neurol. *20*, 194–202. https://doi.org/10.1097/WCO.0b013e328042baf6.

62. Kim, S., and Mountz, J.M. (2011). SPECT imaging of epilepsy: an overview and comparison with F-18 FDG PET. Int. J. Mol. Imaging *2011*, 813028. https://doi.org/10.1155/2011/813028.

63. Boscolo Galazzo, I., Mattoli, M.V., Pizzini, F.B., De Vita, E., Barnes, A., Duncan, J.S., Jäger, H.R., Golay, X., Bomanji, J.B., Koepp, M., et al. (2016). Cerebral metabolism and perfusion in MR-negative individuals with refractory focal epilepsy assessed by simultaneous acquisition of (18)F-FDG PET and arterial spin labeling. Neuroimage Clin. *11*, 648–657. https://doi.org/10.1016/j.nicl.2016.04.005.

64. Leal-Campanario, R., Alarcon-Martinez, L., Rieiro, H., Martinez-Conde, S., Alarcon-Martinez, T., Zhao, X., LaMee, J., Popp, P.J.O., Calhoun, M.E., Arribas, J.I., et al. (2017). Abnormal capillary vasodynamics contribute to ictal neurodegeneration in epilepsy. Sci. Rep. *7*, 43276. https://doi.org/10.1038/srep43276.

65. Sloviter, R.S., and Bumanglag, A.V. (2013). Defining "epileptogenesis" and identifying "antiepileptogenic targets" in animal models of acquired temporal lobe epilepsy is not as simple as it might seem. Neuropharmacology *69*, 3–15. https://doi.org/10.1016/j.neuropharm.2012.01.022.

66. Morkavuk, G., Koc, G., and Leventoglu, A. (2021). Is the differential diagnosis of epilepsy and psychogenic nonepileptic seizures possible by assessing the neutrophil/lymphocyte ratio? Epilepsy Behav. *116*, 107736. https://doi.org/10.1016/j.yebeh.2020.107736.

67. Güneş, M., and Büyükgöl, H. (2020). Relationship between generalized epileptic seizure and neutrophil/lymphocyte ratio, platelet/lymphocyte ratio, and neutrophil mediated inflammation. Int. J. Neurosci. *130*, 1095–1100. https://doi.org/10.1080/00207454.2020.1722662.

68. Özdemir, H.H., Akil, E., Acar, A., Tamam, Y., Varol, S., Cevik, M.U., and Arikanoglu, A. (2017). Changes in serum albumin levels and neutrophil-lymphocyte ratio in patients with convulsive status epilepticus. Int. J. Neurosci. *127*, 417–420. https://doi.org/10.1080/00207454.2016.1187606.

69. Ohira, J., Yoshimura, H., Morimoto, T., Ariyoshi, K., and Kohara, N. (2019). Factors associated with the duration of the postictal state after a generalized convulsion. Seizure *65*, 101–105. https://doi.org/10.1016/j.seizure.2019.01.001.

70. Lehtimäki, K.A., Keränen, T., Huhtala, H., Hurme, M., Ollikainen, J., Honkaniemi, J., Palmio, J., and Peltola, J. (2004). Regulation of IL-6 system in cerebrospinal fluid and serum compartments by seizures: the effect of seizure type and duration. J. Neuroimmunol. *152*, 121–125. https://doi.org/10.1016/j.jneuroim.2004.01.024.

71. Lehtimäki, K.A., Keränen, T., Palmio, J., Mäkinen, R., Hurme, M., Honkaniemi, J., and Peltola, J. (2007). Increased plasma levels of cytokines after seizures in localization-related epilepsy. Acta Neurol. Scand. *116*, 226–230. https://doi.org/10.1111/j.1600-0404.2007.00882.x.

72. Sinha, S., Patil, S.A., Jayalekshmy, V., and Satishchandra, P. (2008). Do cytokines have any role in epilepsy? Epilepsy Res. *82*, 171–176. https://doi.org/10.1016/j.eplepsyres.2008.07.018.

73. Lee, S.J., and Benveniste, E.N. (1999). Adhesion molecule expression and regulation on cells of the central nervous system. J. Neuroimmunol. *98*, 77–88. https://doi.org/10.1016/s0165-5728(99)00084-3.

74. Han, K., Lee, M., Lim, H.K., Jang, M.W., Kwon, J., Lee, C.J., Kim, S.G., and Suh, M. (2020). Excitation-inhibition imbalance leads to alteration of neuronal coherence and neurovascular coupling under acute stress. J. Neurosci. *40*, 9148–9162. https://doi.org/10.1523/JNEUROSCI.1553-20.2020.

75. Berthiaume, A.A., Hartmann, D.A., Majesky, M.W., Bhat, N.R., and Shih, A.Y. (2018). Pericyte structural remodeling in cerebrovascular health and homeostasis. Front. Aging Neurosci. *10*, 210. https://doi.org/10.3389/fnagi.2018.00210.

76. Lee, S., Kang, B.M., Kim, J.H., Min, J., Kim, H.S., Ryu, H., Park, H., Bae, S., Oh, D., Choi, M., and Suh, M. (2018). Real-time in vivo two-photon imaging study reveals decreased cerebro-vascular volume and increased blood-brain barrier permeability in chronically stressed mice. Sci. Rep. *8*, 13064. https://doi.org/10.1038/s41598-018-30875-y.

77. Bracko, O., Vinarcsik, L.K., Cruz Hernández, J.C., Ruiz-Uribe, N.E., Haft-Javaherian, M., Falkenhain, K., Ramanauskaite, E.M., Ali, M., Mohapatra, A., Swallow, M.A., et al. (2020). High fat diet worsens Alzheimer's disease-related behavioral abnormalities and neuropathology in APP/PS1 mice, but not by synergistically decreasing cerebral blood flow. Sci. Rep. *10*, 9884. https://doi.org/10.1038/s41598-020-65908-y.

78. Shih, A.Y., Friedman, B., Drew, P.J., Tsai, P.S., Lyden, P.D., and Kleinfeld, D. (2009). Active dilation of penetrating arterioles restores red blood cell flux to penumbral neocortex after focal stroke. J. Cerebr. Blood Flow Metabol. *29*, 738–751. https://doi.org/10.1038/jcbfm.2008.166.

79. Kleinfeld, D., Mitra, P.P., Helmchen, F., and Denk, W. (1998). Fluctuations and stimulus-induced changes in blood flow observed in individual capillaries in layers 2 through 4 of rat neocortex. Proc. Natl. Acad. Sci. USA *95*, 15741–15746. https://doi.org/10.1073/pnas.95.26.15741.

80. Schaffer, C.B., Friedman, B., Nishimura, N., Schroeder, L.F., Tsai, P.S., Ebner, F.F., Lyden, P.D., and Kleinfeld, D. (2006). Two-photon imaging of cortical surface microvessels reveals a robust redistribution in blood flow after vascular occlusion. PLoS Biol. *4*, e22. https://doi.org/10.1371/journal.pbio.0040022.

81. Gao, Y.R., and Drew, P.J. (2014). Determination of vessel cross-sectional area by thresholding in Radon space. J. Cerebr. Blood Flow Metabol. *34*, 1180–1187. https://doi.org/10.1038/jcbfm.2014.67.

82. Drew, P.J., Blinder, P., Cauwenberghs, G., Shih, A.Y., and Kleinfeld, D. (2010). Rapid determination of particle velocity from space-time images using the Radon transform. J. Comput. Neurosci. *29*, 5–11. https://doi.org/10.1007/s10827-009-0159-1.

83. Chhatbar, P.Y., and Kara, P. (2013). Improved blood velocity measurements with a hybrid image filtering and iterative Radon transform algorithm. Front. Neurosci. *7*, 106. https://doi.org/10.3389/fnins.2013.00106.

84. Shih, A.Y., Driscoll, J.D., Drew, P.J., Nishimura, N., Schaffer, C.B., and Kleinfeld, D. (2012). Two-photon microscopy as a tool to study blood flow and neurovascular coupling in the rodent brain. J. Cerebr. Blood Flow Metabol. *32*, 1277–1309. https://doi.org/10.1038/jcbfm.2011.196.

STAR★METHODS

KEY RESOURCES TABLE

REAGENT or RESOURCE	SOURCE	IDENTIFIER
Antibodies		
Alexa Fluor 488-conjugated Ly6C/G (Gr-1) antibody	eBioscience	Cat# 53-5931-82; RRID: AB_469918
Anti-Ly6G antibody	BD Bioscience	Cat#551459; RRID: AB_394206
Rat IgG2a	BD Bioscience	Cat#559073; RRID: AB_479682
Anti-ICAM-1	Abcam	Cat#ab179707; RRID: AB_2814769
Anti-VCAM-1	Abcam	Cat#ab134047; RRID: AB_2721053
Anti-CD62P	Abcam	Cat#ab59738; RRID: AB_940914
Anti-CD62E	Abcam	Cat#ab18981; RRID: AB_470289
Anti-GAPDH	Abcam	Cat#ab9485; RRID: AB_307275
Goat anti-rabbit IGG H&L, HRP conjugated	Abcam	Cat#ab6721; RRID: AB_955447
Chemicals, peptides, and recombinant proteins		
Urethane	Sigma-Aldrich	U2500; CAS: 51-79-6
4-aminopyridine	Sigma-Aldrich	275875; CAS: 504-24-5
Hoechst 33342	Invitrogen	Cat#H3570; CAS: 23491-52-3
Texas Red-conjugated 70 kDa dextran	Invitrogen	Cat#D1830
Texas Red-conjugated lysine-fixable dextran	Invitrogen	Cat#D1822
4′,6-diamidino-2-phenylindole (DAPI)	Sigma-Aldrich	Cat#D9542; CAS: 28718-90-3
Vectashield HardSet Antifade Mounting Medium	Vector Laboratories	Cat#H-1400-10
Experimental models: Organisms/strains		
Mouse: wild-type C57BL/6N	Orient Bio, South Korea	N/A
Mouse: wild-type C57BL/6N	Japan SLC, Inc	N/A
Software and algorithms		
MATLAB	Mathworks	N/A
ImageJ version 1.53	ImageJ Software	N/A
Other		
Glass capillary tube	Sutter Instrument	Cat#BF100-50-10

RESOURCE AVAILABILITY

Lead contact

Further information and requests for resources should be directed to and will be fulfilled by the lead contact, Minah Suh (minahsuh@skku.edu).

Materials availability

This study did not generate new unique reagents.

Data and code availability

- Data reported in this paper will be shared by the lead contact upon reasonable request.
- This paper does not report original code.
- Any additional information required to reanalyze the data reported in this paper is available from the lead contact upon request.

EXPERIMENTAL MODEL AND SUBJECT DETAILS

Animals

All experimental procedures were approved by the Institutional Animal Care and Use Committee (IACUC) of Sungkyunkwan University (SKKU). The procedures were conducted in accordance with the Guide for the Care and Use of Laboratory Animals of the Animal Protection Law and the Laboratory Animal Act set by the Korea Animal and Plant Quarantine Agency and the Korea Ministry of Food and Drug Safety. Eight-week-old male C57BL/6N mice (22–24 g, purchased from Orient Bio, South Korea & Japan SLC, Inc.) were used. Mice were housed under a 12-h dark/light cycle, with a temperature of 24–25°C and 50–60% humidity.

Experimental design

All experiments were carried out on 10- to 14-week-old C57BL/6N male mice. A total of 105 mice were included in the study: 28 mice for *in vivo* CBF measurements (control n = 6, seizure n = 6, seizure with antibody treatments n = 16), 41 mice for *in vivo* vessel imaging experiments (control n = 9, seizure n = 14, seizure with antibody treatments n = 18), 18 mice for confocal imaging of fixed brain tissues (control n = 4, seizure n = 5, seizure with antibody treatments n = 9), 18 mice for western blotting experiments (control n = 9, seizure n = 9). The study design and reporting followed the ARRIVE (Animal Research: Reporting *In Vivo* Experiments) guidelines.

METHOD DETAILS

Animal preparation

Mice were initially anesthetized with 2.5% isoflurane. Once the mice were transferred to a stereotaxic frame (Kopf Instruments, USA), anesthesia was maintained with 1.2–1.5% isoflurane. Body temperature was maintained at approximately 37°C by using a temperature-controlled heating pad (DC temperature control system, FHC). An incision was made in the skin over the right hemisphere, where a 2-mm diameter circular craniotomy was performed over the somatosensory cortex (0.5–2.5 mm posterior to the bregma and 1–3 mm lateral to the midline) using a dental drill (Ram Products, Microtorque II, USA). The dura mater remained intact, and the exposed cortex was hydrated with HEPES-buffered saline (135 nm NaCl, 5 mM KCl, 10 mM HEPES, 10 mM glucose, 2 mM $CaCl_2$, 2 mM $MgSO_4$). The exposed cortex was covered with a glass cover slip (4 × 4 mm, Deckglaser, Germany), but a partial opening was left on the lateral side to allow for insertion of a microelectrode and a glass pipette, as described in our previous studies.[36,74] A metal holding frame was then attached to the skull to minimize head motions during data acquisition. Anesthesia was switched to urethane (1.25 g/kg, i.p.) for further experiments as depicted in Figure 1A. Throughout the experiments, physiological parameters (heart rate: 550–650 bpm, SpO_2: 98–99%, and respiratory rate: 165–180 r/min) were continuously monitored with a paw sensor (PhysioSuite, Kent Scientific, USA).

Seizure model establishment and electrophysiology

For the induction of epileptic seizures via intracortical injection of 4-AP (15 mM in sterile saline, 420 nl; Sigma, USA), a glass micropipette with a tip diameter of 15–20 μm was made from a glass capillary tube (outer diameter: 1.0 mm, inner diameter: 0.5 mm, borosilicate glass; Sutter Instrument, USA). A tungsten microelectrode (300–500 kΩ, FHC, USA) was used for local field potential (LFP) recordings to verify seizure events. A glass pipette filled with the 4-AP solution, and a microelectrode were carefully inserted into layer 2/3 of the somatosensory cortex. The distance between the glass pipette and the microelectrode tip was approximately 500 μm in all experiments. Raw electrophysiological data were amplified and acquired at 40000 Hz (Omniplex, Plexon, USA). The data were downsampled to 1000 Hz and filtered with 0.5 Hz high-pass and 200 Hz low-pass filters to acquire LFP signals.

CBF recording by laser Doppler flowmetry (LDF)

CBF signals were measured by using an LDF probe (wavelength: 780 nm, probe diameter: 450 μm, Perimed, Periflux System 5000, Sweden). The tip of the LDF probe was located between the LFP recording microelectrode and the pipette, avoiding large pial vessels. The signals measured from the LDF probe were sampled at ~20 Hz and digitized through a Plexon system that enabled simultaneous data acquisition with the LFP recordings. LDF signals were continuously measured from the 10-min baseline (before the 4-AP injection) to 1–1.5 hr after the end of the seizure events.

Two-photon vasculature imaging

A 10× water immersion objective lens (10×/0.3NA, Leica) coupled with a CCD camera was used to navigate through the brain surface and acquire surface vessel imaging data. Two-photon imaging was performed with a 25× water immersion objective lens (25×/0.95 NA, Leica) in a two-photon laser scanning microscopy system (TCS SP8 MP, Leica, Germany) with a broadly tunable Ti:sapphire laser (680–1080 nm, 80 MHz, 140 fs pulse width; Chameleon Vision II, Coherent, USA). To visualize cortical vessels, Texas Red-conjugated dextran (70 kDa, Thermo Fisher Scientific, USA) was injected via the retro-orbital sinus (5% in PBS, 1.5 μl/g). Vasculature images were acquired at a 0.693 μm/pixel resolution. In some animals, neutrophils and nuclei were further stained via retro-orbital injection of an Alexa Fluor 488-conjugated Ly6C/G (Gr-1) antibody (0.12 mg/kg)[44] and Hoechst 33342 (50 μl, 4.8 mg/ml in 0.9% saline; Thermo Fisher Scientific).[41,42] A 920-nm tuned laser was used to excite Texas Red fluorescence. An 800-nm tuned laser was used for Alexa Fluor 488 and Hoechst 33342. Bandpass filters at 460/50 nm, 520/50 nm and 620/40 nm were used to acquire the emitted fluorescent signals of Hoechst 33342, Alexa 488, and Texas Red, respectively. Red blood cell (RBC) movements are shown as dark streaks within the fluorescently labeled blood plasma. Each vessel segment with dark streaks was replenished by this averaging method. To visualize the cortical vasculature, stacks of images spaced at 1 μm axially were sequentially acquired (~375 ms per each plane) from the cortical surface to a cortical depth of 300 μm. Vascular imaging was conducted one hour after the last seizure terminated.

RBC velocity

To measure capillary blood flow, RBC velocity was measured at vessel segments above the 4th branch order from penetrating arterioles.[39,75] The branch order was counted by tracing vessel segments from a penetrating arteriole (0th branch order) and increasing the count by 1 for each subsequent bifurcation. Due to the presence of Texas Red-conjugated dextran, RBCs appeared as dark segments in a line of brightly labeled plasma in the vessel lumen. The motion of the dark segments indicates flowing RBCs. To create space-time images with RBC streaks, high-resolution line-scan images at a scan rate of 2 kHz and a 0.138 μm/pixel resolution were collected along the centerline of a vessel segment over a length of 512 pixels, which was approximately 80 μm. In each segment, line-scan imaging was conducted for 1–5 min.

Neutrophil staining and confocal microscopy imaging

A different subset of experiments was conducted to quantify neutrophil stalling in brain capillaries. One hour after the end of seizures, a mixture of Texas Red-conjugated lysine-fixable dextran (70 kDa, 5% in PBS, 1.5 μl/g) and an Alexa Fluor 488-conjugated Ly6C/G (Gr-1) antibody (0.12 mg/kg) was administered via the retro-orbital sinus. After 30 minutes, the mouse brain was extracted and then postfixed with 4% paraformaldehyde (PFA) overnight at 4°C. The brain was then sectioned with a vibratome (VT 1200S, Leica, Germany) to obtain 100-μm-thick coronal sections. Three coronal sections were chosen in each mouse: one at the same coronal coordinate as the 4-AP injection focus and the others at 200- or 300-μm anterior and posterior to the focus. Cell nuclei were stained with 4′,6-diamidino-2-phenylindole (DAPI, Sigma, 1:10000). Fluorescence images were captured using a confocal laser microscope (TCS SP8, Leica) equipped with a 40x (40x/1.1NA, Leica) water immersion objective. A 405-nm diode laser was used to excite DAPI signals, and 488- and 595-nm tuned lasers were used to excite Alexa 488 and Texas Red fluorescence.

Antibody treatment

Monoclonal antibodies against lymphocyte antigen 6 complex, locus G (Ly6G) (α-Ly6G antibody (clone 1A8, 2 mg/kg, BD Biosciences, USA)[41–43] were administered intravenously 40 minutes prior to 4-AP injection. In another group of animals, isotype control antibody (Rat IgG2a, κ, 2 mg/kg, BD Biosciences) was injected as the control. Animals were randomized into treatment groups before the experiments. Another group of mice was treated with an intravenous injection of monoclonal antibodies against leukocyte function- associated antigen-1 (α-LFA-1; clone M17/4, 2 mg/kg, BD Biosciences) 40 minutes prior to the 4-AP injection.

Western blotting

Brain tissues around the 4-AP injection site (1.5 mm × 1.5 mm x 1 mm) were prepared in RIPA lysis buffer (Biomax, South Korea) containing a universal protease inhibitor cocktail (Biomax) and maintained at 4°C for 1 h. The lysates were centrifuged at 12700 rpm for 20 min at 4°C. Thereafter, the supernatant was carefully collected, and the protein concentration was determined using a BCA protein assay kit (Thermo Fisher

Scientific, USA). Twenty micrograms of protein from each sample was loaded and resolved on a 10% mini-PROTEAN TGX gel (Bio-Rad, USA) in Tris/glycine/SDS buffer (Bio-Rad). The proteins were transferred to PVDF membranes (Bio-Rad) using a Trans-Blot Turbo transfer system (Bio-Rad). After blocking with EveryBlot blocking buffer (Bio-Rad) for 30 min at room temperature, the membranes were incubated overnight at 4°C with primary antibodies against the following proteins: intercellular adhesion molecule-1 (ICAM-1; 1:500, ab179707, Abcam, UK), vascular cell adhesion molecule-1 (VCAM-1; 1:1000, ab134047, Abcam), CD62P (P-selectin; 1:300, ab59738, Abcam), CD62E (E-selectin; 1:500; ab18981, Abcam), and glyceraldehyde 3-phosphate dehydrogenase (GAPDH; 1:10000; ab9485, Abcam). The membranes were washed four times with TBS buffer (Bio-Rad) containing 0.1% Tween-20 (Bio Basic Inc., Canada). Then, the membranes were incubated with the appropriate horseradish peroxidase-conjugated secondary antibody for 1 h at room temperature. The proteins were detected using an enhanced chemiluminescence (ECL) substrate (Bio-Rad) and a ChemiDoc XRS+ system (Bio-Rad). The band intensity was calculated with ImageJ, and the amounts of the target proteins were normalized to GAPDH, which was used as a loading control.

QUANTIFICATION AND STATISTICAL ANALYSIS

All image processing was carried out using Fiji (ImageJ, NIH, US) and MATLAB (MathWorks, USA). LFP data were analyzed by using Chronux, an open-source software package for the analysis of neural data (available at http://chronux.org/).

CBF change

The LDF data were downsampled to 10 Hz and averaged in each 5 s sliding window. The measured LDF signals were then normalized to the averaged values from the 10-min baseline period to calculate CBF changes. ΔCBF (%)=(CBF/CBF_0 -1)x100, where CBF_0 and CBF represent the average baseline value and the signal values over time, respectively.

Vessel diameter

Image preprocessing and diameter mapping were conducted as previously described.[76] For each vessel segment, the diameter was calculated via Euclidian distance transformation of the fitted sphere located at the center point of vasculature images that were converted to binary. This process generated a diameter map for each vessel. To compare vessel diameters at the same coordinate, each diameter map for the post-saline or the postictal data was registered to its corresponding baseline diameter map using nonrigid 3D transformation. The diameter maps were then skeletonized and converted into a network graph based on a 26-cell cubic neighborhood. Microvessels smaller than 10 μm were generally classified as capillaries.[40–42]

Quantification of flowing and nonflowing vessel segments

To evaluate capillary flow, 1- or 2-μm spaced image stacks were acquired at ~1.5 seconds per frame, such that each capillary segment was visible for a minimum of ~5 seconds.[40,42,77] Capillaries were defined as stalled if a dark patch in the vessel lumen did not move over the observation time for that capillary segment.[77] When one segment had several stalls, it was counted as one.

RBC velocity and flux

RBC velocity was calculated from the slope angle of the line-scan streaks.[78–80] The Radon transform was applied to the line-scan images,[81,82] which were preprocessed with a Sobel filter to enhance image contrast for accurate calculation of the velocity.[83] RBC streaks were quantified from the data for every 400-ms image. The RBC velocity in a vessel segment was calculated by averaging the velocities for 1–5 min of imaging data. For RBC volume flux measurements, the capillary diameter and RBC velocity collected from a single vessel were used to define the RBC volume flux, $\vec{F}$, as follows:

$$\vec{F} = \frac{\pi}{8}\vec{v}(0)d^2$$

where $\vec{v}(0)$ is the RBC velocity and d is the lumen diameter, with the assumption that the flow in the capillary is laminar.[78,84]

LFP data

The 4-AP injection reliably induced recurrent spontaneous seizures that repeatedly occurred at intervals of several tens of seconds to several minutes. The duration during which recurrent seizures were maintained

was referred to as the "seizure duration" in this study. The termination of seizure events was determined as the time point at which the LFP signals no longer exceeded five standard deviations (SD) above the pre-injection baseline. Termination of the seizure event was then confirmed by visual inspection. To compare the strength of seizure activities in three different groups (4-AP vs. cIgG+4-AP vs. αLy6G+4-AP), coastline length was calculated. This referred to the absolute values of the distances from one data point to the next.[37,38] From the time point of the 4-AP injection to the seizure end-time, the coastline length was calculated and summed. Spectral power during the postictal period was calculated by applying a multitaper transformation.

Statistics

In this study, box-and-whisker plots show the 25-75th percentiles of the data, with the whiskers extending to 1.5 times the difference between the values of the 25th and 75th percentiles. The median is indicated by a black horizontal line inside the box. Bar plots show the mean $\pm$ standard deviation (SD). A normal distribution of the data was validated with either the Shapiro–Wilk test ($n < 50$) or Kolmogorov–Smirnov test ($n \geq 50$) using SPSS (IBM SPSS statistics 19, USA). Parametric statistics were used when the data in all groups in the comparison were normally distributed. Otherwise, nonparametric tests were used. Either an independent *t* test or the Mann–Whitney *U* test was used to examine differences between two independent samples. One-way ANOVA or Kruskal–Wallis *H* test was used with the Bonferroni correction for multiple comparisons. Likewise, either Pearson's or Spearman's correlation coefficient was used to evaluate the linear relationship between two variables. Linear regression models were fitted using the ordinary least squares method. Details including the number of animals, number of vessel segments and *p* values are included in the figure legends.